Adaptive Joint Source-Channel Coding of Real-Time Multimedia for Cognitive Radio

by

Aditya Kedia

A Thesis

submitted to the Faculty of Graduate Studies of The University of Manitoba,

in partial fulfilment of the requirements for the degree of

Master of Science

Department of Electrical and Computer Engineering

University of Manitoba

Winnipeg, Manitoba R3T 5V6 Canada

Abstract

Radio spectrum has become a scarce and priced resource due to the rapid growth of wireless networks. However, recent surveys conducted by the FCC indicate that a large part of the allotted frequency spectrum lies unused. Cognitive radio systems, built on the software defined radios, allow the efficient usage of these unused frequency spectrum. Cognitive radio systems can be modeled as a multiple access channel in which certain users have the priority (primary users) while others (cognitive or secondary users) are allowed to access the channels without causing any interference to the primary users. However a secondary user's transmissions not only encounter high levels of uncertainty and variability in the number of channels available to them, but they also suffer data losses if a primary user activity occurs. Under such rigid constraints, the reliable transmission of real time multimedia of a secondary user with an acceptable quality of service becomes challenging.

Multimedia transmission in a cognitive system requires channel adaptive source and channel coding schemes. In order to address this problem, this thesis investigates and develops a novel joint source-channel coding (JSCC) approach. The proposed JSCC allows the dynamic generation of codes, which minimizes the end-to-end distortion. This JSCC is based on quantized frame expansions to introduce redundancy into transmitted data. An algorithm has been developed to determine the optimal trade-off between redundancy and quantization rate, under a constraint on channel capacity. The proposed approach does not require the communication of any overhead data between the transmitter and receiver. When compared to codes commonly used to deal with packet losses, simulation results indicate that the proposed JSCC can achieve lower distortion for secondary user's transmissions in cognitive radio systems.

Acknowledgements

First and foremost, I would like to thank and express my deepest gratitude to my advisor, Dr. Pradeepa Yahampath. It would not have been possible for me to come so far without his excellent guidance, support and encouragement. His invaluable assistance and patience have truly been inspirational and helped me further my enthusiasm towards research work. My sincere gratitude to the professors in as well as outside the department for helping me improve my knowledge and understanding in numerous ways.

I would also like to thank the administrative staff of the Faculty of Graduate Studies and the department of Electrical and Computer Engineering. A special thank to our graduate advisor, Ms. Amy Dario, for her constant help and support. My experience as a masters student would have been incomplete without my friends at the University whose help and support was invaluable.

Lastly, the most important people in my life, my family- my sister, my wife and my parents . Their support, love and dedication has been a driving force for me. I cannot thank them enough for all that they have done for me. I would like to dedicate this thesis to my beloved family.

Contents

List of Tables

List of Figures

List of Abbreviations

SU	Secondary user
PU	Primary user
TDMA	Time division multiplexed access
JSCC	Joint source channel coding
MDC	Multiple description coding
CORVUS	Cognitive radio for virtual unlicensed spectrum
LT	Luby transform
SPIHT	Set partition in hierarchical trees
PET	Priority encoding transmission
FEC	Forward error correction
MSE	Mean squared error
BOV	Block of vectors
RTS	Request-to-send
CTS	Clear-to-send
PSNR	Peak signal-to-noise ratio

List of Notations

K	Dimensionality of the source vector
n	Number of source vectors per transmission
t	Time instance for transmission
j	Index for BOV, where $j = 0, \cdots, n-1$
$N_{t,j}$	Expansion factor
R	Sampling or data generation rate
β_t	Number of PU channels available for transmission
r_S	Number of bits available per sample
l	Packet length in bits
h	Number of bits allocated to the header
L_t^{max}	Maximum number of packets that can be generated
L_t	Number of packets that can be transmitted
M_t^{min}	Minimum number of channels required for L_t^{max} packets to be transmitted
M_t	Number of channels user for transmission
T_p	Time per packet
C	Channel capacity
i	Channel index, where $i = 1, \cdots, M_t$
λ_i	PU arrival rate on channel i
T_i	Random variable denoting time on channel i
η_i	Number of packets received on channel i
$P_{packets}$	Probability of receiving packets on a particular channel

f_{T_i}	PDF for inter-arrival time
$\bar{\eta}$	Total number of packets received
P_{total}	Probability of receiving packets over all channels
$P_{tj}(c)$	Probability of receiving c coefficients of the source vector j
$b_{t,j}$	Bit allocated to each coefficient of the source vector j
$\underline{X}_{tj}$	Original data transmitted at time t belonging to the source vector j
$\underline{\hat{X}}_{tj}$	Estimation of data transmitted at time t belonging to the source vector j
$D_q(b_{t,j})$	Distortion produced by a quantizer for the bit rate $b_{t,j}$
e	Number of erasures
D_{tj}	Distortion induced for the source vector j at time t
D_{BOV}	Distortion induced for the BOV
D_F	Distortion induced for the entire source vector
σ_j^2	Variance of source vector j
$\underline{X}$	The entire data transmitted
$\underline{\hat{X}}$	Estimated value for data transmitted

Chapter 1

Introduction

There is an ever-increasing demand for radio spectrum, which has now become a scarce resource due to the proliferation of wireless systems and services. However, recent studies [3] [4] have revealed that large portions of licensed radio spectrum are underutilized. This has motivated the development of new spectrum allocation policies to better utilize the radio spectrum. Bands of underutilized or unused frequencies at any particular time and geographical location are termed as *spectrum holes* [5, 6]. Cognitive radio [7] is an emerging approach which aims to improve the spectrum utilization by sensing the spectrum holes, and re-allocating them to various wireless users. Cognitive radio systems use the network information along with the regulatory constraints to make their decision on whether to *underlay, overlay or interweave* [8] the signals with those of the licensed users such that the communication of the licensed users is not significantly impacted.

- *Underlay*

  The underlay paradigm assumes that an unlicensed secondary user (SU) has the knowledge of the interference caused by its transmitter at the licensed primary user's (PU) receiver. The underlay paradigm thereby allows the concurrent/simultaneous transmission of signals from PUs and SUs under the condition that the interference caused by the SU transmitters at the PU receivers is below an acceptable threshold.

- *Overlay*

  Contrary to the underlay paradigm, the overlay paradigm assumes that SUs have the knowledge of the channel gains, the codebook and the message being sent out by a PU. The SUs transmit concurrently with the PUs at any power and the interference caused by the SUs is offset by using the SUs power to relay the message from the PU.

- *Interweave*

  The interweave paradigm requires the SUs to have the knowledge of PU activities in the spectrum. This allows the SUs to sense the radio environment in order to make informed decisions to utilize spectrum holes or white spaces in a non-interfering manner with respect to the PU transmissions. The SUs, therefore, monitor the radio spectrum, detect the spectrum holes and then communicate over these spectrum holes.

The underlay and overlay paradigms allow SUs to transmit simultaneously with the PUs, however, a SU must ensure that the interference to the PU is kept below a prescribed threshold. This can be seen as transmission across multiple-access channels with interferences, a simple model for which is the Gaussian interference channel [8], widely studied in information theory.

On the other hand, in the interweave paradigm, SUs are allowed to access a frequency-band only when the designated PU is not transmitting on it, which amounts to an opportunistic (random) time division multiplexed access (TDMA) [9] from the SU's perspective as shown in Figure 1.1. With the interweave paradigm, the main objective of *source and channel coding* [2] by a SU is to ensure a certain minimum level of reconstruction quality, under the uncertainties of the cognitive radio environment (discussed in Section 1.1). In this thesis, an approach to reliable multimedia transmission over cognitive radio network based on interweave paradigm is developed.

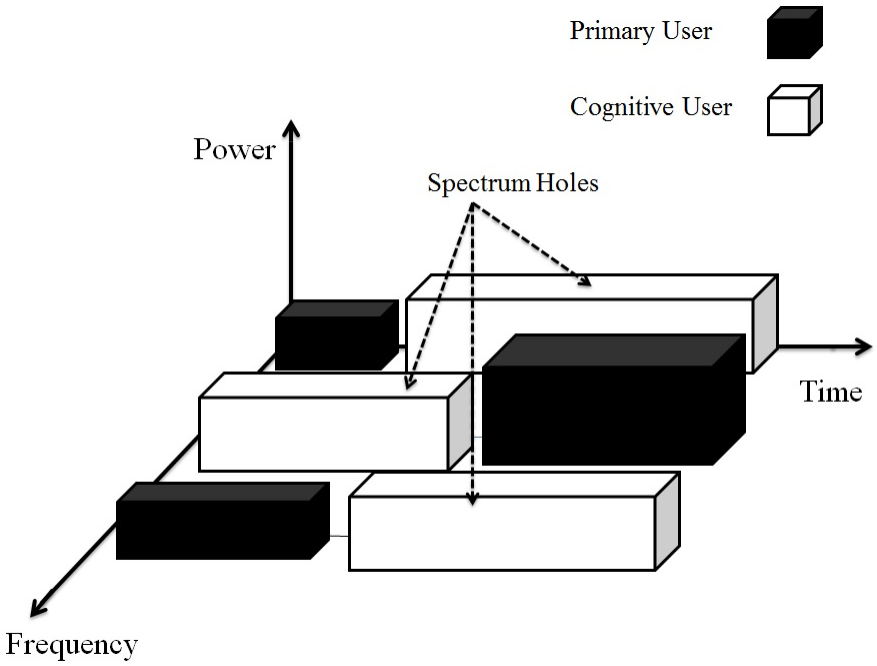

Figure 1.1: TDMA view of cognitive radio network.

1.1 Challenges in Real Time Cognitive Radio Communication for a SU

In a cognitive radio network, SU transmissions would not only encounter high levels of uncertainty and variability in the number of channels available to them but would also suffer data loss if a PU activity was to occur. Under such rigid constraints and without any room for re-transmission of missing data, the reliable transmission of real time multimedia over the cognitive radio network with an acceptable quality of service becomes challenging. The main challenges of transmitting any form of data in such conditions are as follows.

1. *Number of available channels* : When using the interweave paradigm, SU transceivers have to sense and use the spectrum holes to communicate their data. Therefore, the number of channels that would be available to a SU for transmission would vary from time to time. As a result, the bit-rate available to a SU varies with time, requiring adaptive coding of the data to match the bit rate to the available channel capacity.

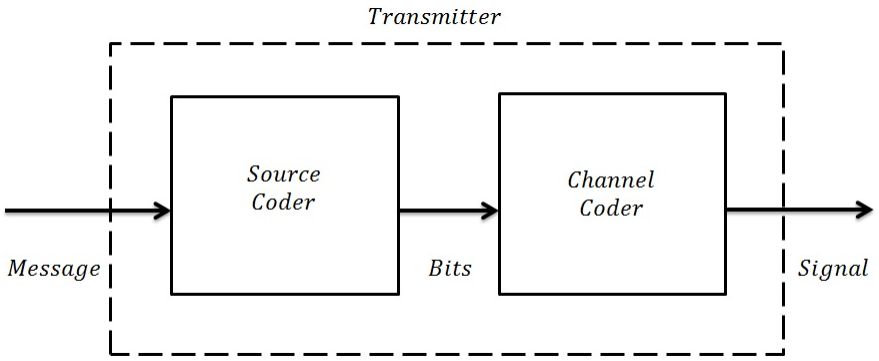

Figure 1.2: Separation of *transmitter* into source coder and channel coder [1]

2. *Erratic PU arrivals & Unpredictable Packets Losses* : Under the interweave paradigm, SU transmissions are not allowed to interfere with PU transmissions. Hence, to counter the unpredictable data loss due to the erratic PU arrivals, some form of compensation needs to be accounted for by the SU transmitter.

3. *Difficulties in retransmission* : Real time transmission leaves no room for retransmission of missing data. To add to that, the cognitive radio environment does not guarantee that a channel would be available for sending an acknowledgement signal back to the transmitter. Without some form of response from the receiver, the transmitter is oblivious to the any losses that occur during transmission [10]. For real-time applications, a SU transmitter should thus be designed with the knowledge that data retransmission is impermissible.

1.2 Issues in Source and Channel Code Design for SU Transmitters

Claude Shannon's remarkable work [2] allowed the characterization of a source and a channel. This further enabled the separation of the transmitter or encoder into two components: a *source* coder and a *channel* coder (See fig. 1.2). While a source coder generates a *compressed version* of the source, a channel coder is used to generate a transmitting signal such

that the compressed version of the source can be conveyed to the receiver with a small error of probability [1]. Given the challenges in cognitive radio transmission described above, the source coder and the channel coder of the SU should exhibit the following properties.

1. The transmission bit rate must be adapted to match the number of available channels and their capacities. The SU source coder should therefore be adaptive in nature, allowing different levels of compression based on the channel conditions. The process of joint source channel coding (JSCC) [11] allows the incorporation of the channel model into the source coder design. In this thesis, an adaptive JSCC coding scheme is developed for real time multimedia transmission.

2. The source information must be encoded into multiple packets which are transmitted over different cognitive radio channels. With unpredictable losses, the reception of all transmitted data packets is not guaranteed and with no scope for retransmission, the source data should be recoverable even if only a subset of the transmitted packets is received. The problem of encoding a source into multiple codewords is known as multiple description coding(MDC) problem [12].

Like many other communication technologies, MDC also had its inception at the Bell Laboratories. It was invented with regards to communicating speech over the telephone network. In its simplest form, the MDC problem requires that the source be described using two descriptions at *rates* (number of bits used for describing the source) R_1 and R_2. The descriptions so generated would individually lead to reconstruction of the source with *distortions* (error) D_1 and D_2 respectively. However, if both descriptions were used for reconstruction the resulting distortion $D_0 \leq min(D_1, D_2)$(See sec. 2.2). The MDC problem can be generalised to more than two descriptions [13] [14].

1.3 Coding For Lossy Communication

Error control coding [15] is used to protect information against channel errors by incorporating redundancy into the transmitted bit stream. Consequently, the number of bits used to transmit a source message across the channel is greater than the minimum number of bit required to represent the source message.

Packet losses can be seen as a form of erasure. The application of erasure codes like forward error correction (FEC) require the use of long codewords, which in turn introduces long coding delays. A FEC code provides robustness by placing channel coder output symbols in different packets. Hence, the performance of an FEC becomes dependent on the number of packets being transmitted. On the other hand, with MDC any subset of packets can be used to obtain useful reconstruction of the source message. This would allow the performance to vary gracefully with the number of received descriptions [16] when compared to FEC erasure coding which would exhibit a "cliff effect" [12]. [17] shows that the performance of MDC increases on wireless links with high packet loss probability. Thus, MDC is suitable for networks with packet transmission, where retransmission is not possible, long delays are unacceptable, while the number of packets being transmitted is not too large [12].

There have been earlier works which implement MDC for communication of delay sensitive SU data over a cognitive radio network. In [18], the author investigates the use of MDC by generating two descriptions to negate the interferences caused by the arrival of PU traffic to SU transmissions. The paper models PU arrivals as a Markov process [19] and converts the problem of selecting optimal rate-distortion pairs $\{(R_1, D_1), (R_2, D_2)\}$ into an exhaustive search algorithm based on an expected utility function. The paper presents numerical results for SU transmission of Gaussian source vectors and image transmission. However, the paper is limited to considering SU transmission on either a single channel or across two channels and ignores the possibility of utilising more than two channels that might be available to the SU. Moreover, the exhaustive search algorithm used in [18] only

considers PU interferences to be the cause for packet losses and ignores the packet loss that might occur due to channel imperfections of the cognitive radio network. This would result in additional packets being lost and would significantly degrade the performance of the SU encoder.

A different approach has been taken in [20] where the concept of *link maintenance* in SU communication has been introduced. The paper implements cognitive radio for virtual unlicensed spectrum (CORVUS) [21] and spectrum pooling [22] for recognising subchannels on which SU transmissions can occur. PU arrivals are considered to be time independent while SU losses occur due to PU interferences and packet losses on subchannels. The SU data losses are compensated by the generation of endless meta-content symbols using Luby transform (LT) codes [23] which act as endless multiple descriptions of the source. However, the method uses an entire sub-channel to transmit redundant bits.

The authors in [10] also use the concept of CORVUS and spectrum pooling to define subchannels for SU transmission. They model the PU arrivals process as a Poisson process [24] and use digital fountain codes [25] to distribute the multimedia content over the cognitive radio network and to compensate for losses caused by the PU traffic interference. The study in [10] focuses on optimizing the number of sub-channels required to achieve maximum spectral efficiency and throughput. The decoder would, however, require a bipartite graph representing the encoding scheme used by the fountain codes to decode. Every transmitted packet would thus require the bipartite graph, increasing the overhead. The results in [10] also indicate that the decoding error probability decreases as the number of packets being combined for generating fountain code is increased. Applications where the number of packets being transmitted are not a large number would result in a high decoding error probability. Also the paper does not present any numerical results on the application of the coding scheme to real-time transmission.

Related work has been done in [26] where set partition in hierarchical trees (SPIHT) [27], a progressive encoding scheme is used for generating a base layer and several enhancement layers. The base layer is critical for the media stream to be decoded while

enhancement layers are applied to improve stream quality. The paper makes use of the priority encoding transmission (PET) [28] packetization technique wherein different amounts of error correction bits are added to different descriptions according to their importance. The number of error correction bits to be added is calculated based on the packet corruptions pattern. The authors present numerical results for the application of their technique. However, SPIHT produces a progressive stream of data, wherein the enhancement layers are rendered useless if base layer is not received. The process becomes entirely dependent on the reception of the base layer and would fail if the base layer was not received at the decoding end.

Frames [29] have been used in communication systems as they provide redundancy to mitigate the effects of packet losses [16, 30–32]. In this thesis, frame representations are used as MDC for the transmission of SU data over cognitive radio network. The advantage of implementing frames are three fold. Firstly, unlike other methods of generating MDC such as correlating transforms, multiple description scalar quantizer (MDSQ) [33], which require the computation of the number of descriptions apriori, frames allow the generation of the descriptions on the fly. Secondly, frames facilitate the generation of multiple descriptions of the source data providing robustness to the effect of erasures in a cognitive radio network. Thirdly, the generated descriptions are independent of the order in which they are received at the decoder. Therefore, the use frames allows the distribution of multimedia content over different channels without any need of coordination among the SU channels. Using frames, K source samples are represented using N codewords ($K \leq N$) and transmitted by the encoder. At the receiver/decoder, the original data can be recovered using *any* K codewords with certain distortion. The reception of more than K codewords adds to the reconstruction procedure allowing the decoder to better the output.

1.4 Summary of Contributions

This thesis presents an adaptive JSCC technique for the reliable transmission of multimedia over cognitive radio network. Frames have been used as JSCC. Unlike the works presented in [10, 33], the proposed method adapts to varying number of available channels, variations in channel capacities and packet losses due to PU arrivals during SU transmissions. This thesis presents an optimization procedure which allows the SU transmitter to add redundancy to the source vector, on the fly, without the need to communicate or coordinate the optimization result to the decoder. Numerical analysis for the implementation of the proposed JSCC to Gaussian source vectors and images are also presented in the thesis. The application of the proposed methodology to video transmission has been left as a future work.

1.5 Outline of Thesis

The rest of the thesis is organized as follows. Chapter 2 briefly explains the fundamental concepts and background studies that are relevant to the work presented in this thesis. Chapter 3 presents the derivation of the proposed adaptive JSC decoder. The numerical results along with its implication are presented in Chapter 4. Chapter 5 concludes the thesis with consideration to possible future work.

Chapter 2

Background

"The fundamental problem of communication is that of reproducing at one point either exactly or approximately a message selected at another point (fig. 2.1*)"*- Claude Shannon, A Mathematical Theory of Communication.

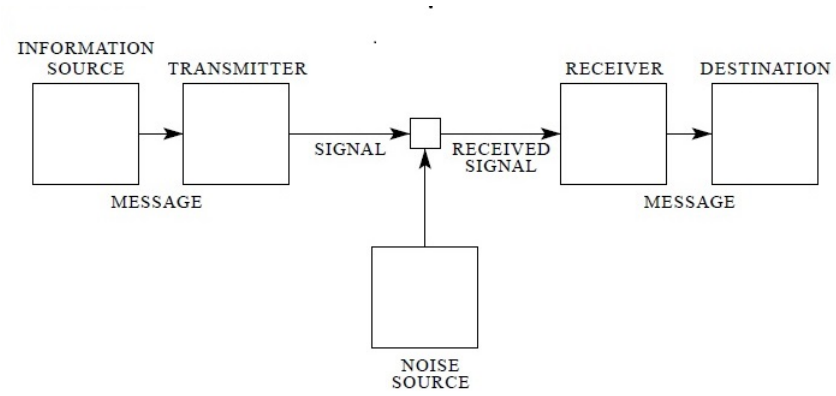

Figure 2.1: Schematic diagram of a general communication system [2].

There are two major challenges when communicating information from one point to another. Firstly, *noise*, which corrupts or causes the complete loss of information and secondly, the *bandwidth limitation* of the channel, which restricts the amount of information that can be transmitted. To ensure reliable communication, error control (channel coding) is applied to the compressed version (source coding) of the information to be transmitted.

We discuss source coding in the following section in order to relate its importance to the developments presented in this thesis. Sec. 2.2 describes multiple description source coding while frames, which are used as MDC has been discussed in sec. 2.3.

2.1 Source Coding

In communication, source coding is the conversion of a signal into an efficient compressed digital representation. Source coding can be classified into two categories:

1. *Noiseless coding* [34] : Lossless or noiseless coding can provide a reduction in the representation of the information by exploiting the statistical redundancy that the information might have. The exact reconstruction of the information source is possible when using lossless coding. Analog sources (voice, video, etc.) cannot be compressed using lossless coding as it would require an infinite number of bits to represent such data accurately.

2. *Lossy coding* : Natural sources of information are continuous in nature. The process of coding an analog signal would necessarily result in distortion since any form of discrete data cannot describe the analog signal in a recoverable manner [34]. The generation of digital representation of information (or bits) from any continuous valued source requires some form of quantization, which is the process of approximating analog signals samples by discrete values.

2.1.1 Quantization

Quantization is one of the most critical steps of lossy source coding. In the words of Gersho and Gray, "Quantization is the heart of analog-to-digital conversion" [34]. A quantizer observes a random value and selects the nearest approximating value according to a predefined rule. The input to a quantizer is usually analog in nature while its output has digital form. The process of quantization can be summed into two distinct mapping operations.

The first mapping being encoding, wherein the input signal is converted to its digital form. The second mapping is known as decoding and is used for the estimation of the original signal from the digital version. Quantization Q can be defined as a mapping Q: $R \rightarrow C$ where R is the real line and and C being the finite output set with $|C| = N$, such that

$$C \equiv \{y_1, y_2, \cdots, y_N\} \subset R \tag{2.1}$$

In any communication system, the process of encoding happens at the transmitter while the decoder operates at the receiver end.

2.1.2 Scalar Quantization

In scalar quantization, the input being digitized is scalar in nature ,$i.e.$, it is usually a real number. The encoder maps this real number onto an integer value. The decoder on the other hand, maps the integer (received over the channel) onto a pre-defined real number from a finite set of possible outputs.

A scalar quantizer with its N output level defining points is shown in fig. 2.2. The values x_i, $i = 1, \ldots, N-1$ define the boundary or decision points. The interval between two successive boundary or decision points forms a region R_i (or a cell). The encoder is thus defined by these successive regions. Each region R_i (or a cell) can be labeled by an integer. If an input value falls into a particular cell or region, it is mapped to the assigned integer. The decoder then maps the encoder output, that is, the integer value onto the corresponding real numbered output y_i.

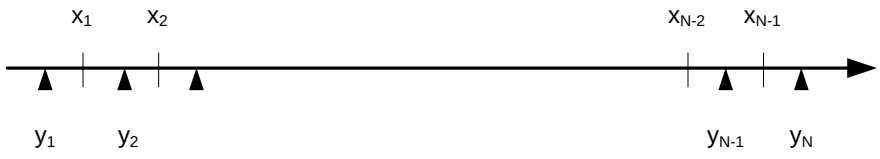

Figure 2.2: Decision points and output levels of an N-point scalar quantizer.

Implementation of a scalar quantizer

The process of quantization provides finite-precision description of a previously unknown input value. As the inputs can not be known in advance, it is necessary to quantize them. Thus, the input can be modeled as a random variable, having a statistical character specified by its probability density function (pdf). Consequently, the distortion produced during the process of quantization can also be viewed as a random variable. With the quantization distortion defined by a statistical model, the average degradation in the quality of the input can be computed as the statistical average of the distortions. In almost all practical scenarios, the mean square error (MSE) [35] is used for measuring the average distortion. For a given input signal, X, where $f_X(x)$ is the probability density function (pdf) of the input and quantizer $Q = \{y_i, R_i; i = 1, 2, \ldots, N\}$, the MSE or the average distortion is given by

$$D = E[(X - Q(X))^2] = \sum_{i=1}^{N} \int_{R_i} (x - y_i)^2 f_X(x)\, dx, \tag{2.2}$$

Uniform quantizer

Uniform quantizers are the most commonly known implementation of quantizers. It has been widely used for general-purpose analog-to-digital conversion. A uniform quantizer is a regular quantizer [34], with the following properties:

1. The boundary/decision points are equally spaced

2. The mid points of the quantization regions are the output levels for each region

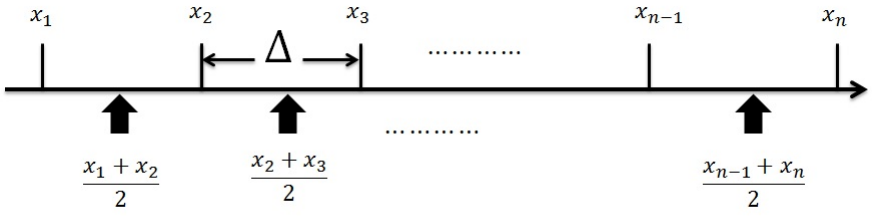

Figure 2.3: Decision points and output levels of an N-point uniform scalar quantizer.

Fig. 2.3 shows the decision points and the corresponding quantization regions for a uniform quantizer. When N is large enough, the overall distortion D for a uniform quantizer is given as [36] [37]

$$D \approx \frac{\Delta^2}{12} \tag{2.3}$$

where Δ is the quantization interval (See fig. 2.3).

Optimal quantizer

Another class of quantizers, known as the optimal quantizers, offer major advantages over uniform quantizers. Firstly, optimal quantizer suitably choose non-uniform spacings or regions, thereby, allowing the dynamic range that can be accommodated for a given resolution to be increased. Secondly, in optimal quantizers, the step sizes and reconstruction levels are so chosen that they minimize the MSE for a given input pdf. Thus, optimal quantizers can yield better performance when compared to uniform quantizers for a specific input pdf and bit resolution [34].

In general, finding a closed-form solution to the quantization design is difficult. With no closed form solutions, [34], provides an iterative optimization of the reproduction levels and the partitions based on the necessary conditions for an optimal quantizer. The two steps in each iteration are,

1. *Determine the optimal encoder for a given set of reproduction levels*:

   The first step requires finding the best partitions for a given set of reproduction values (codebook) that minimize the distortion.

   For a given set of output levels, C, the partition cells satisfy:

   $$R_i \subset x_i : d(x, y_i) \leq d(x, y_j); \text{ for all } j \neq i \tag{2.4}$$

   that is,

   $$Q(x) = y_i; \text{ only if } d(x, y_i) \leq d(x, y_j); \text{ for all } j \neq i \tag{2.5}$$

The nearest neighbour condition is proved as being the optimal solution to this problem in [34]. The nearest neighbour condition requires that a quantization region consists of all input values closer to its reproduction value than to any other reproduction value. Thus,

$$d(x, Q(x)) = \min_{y_i \epsilon C} d(x, y_i) \tag{2.6}$$

The requirement of the nearest neighbour condition can easily be achieved by choosing decision points to be the *midpoint* between two adjacent output levels, *i.e.*

$$x_{i-1} = \frac{(y_{i-1} + y_i)}{2}. \tag{2.7}$$

The nearest neighbour rule fully defines the partition of the quantizer.

2. *Determine the optimal decoder for a given set of partitions*:

   Contrary to the first problem, the requirement here is that of finding the optimal codebook for fixed partitions. Given that MSE is being used as the distortion criteria, the centroid conditions is both the sufficient and necessary condition for the generation of the codebook for an optimal quantizer [34]. The centroid condition simply states that the optimal output level, y_i, for the ith cell of the partition is the *centroid* or the center of mass, of the part of input pdf that lies in the given region R_i.

   Given a partition, the optimal codebook for a given random variable (i.e. the pdf of the input signal) is given by

$$y_i = \int_{R_i} x f_{X|R_i}(x)\, dx = \frac{\int_{R_i} x f_X(x)\, dx}{\int_{R_i} f_X(x)\, dx}. \tag{2.8}$$

In [38], (2.7) and (2.8) are used iteratively, until the average distortion converges to a stationary point. Figure 2.4 illustrates the basic design algorithm presented in [38].

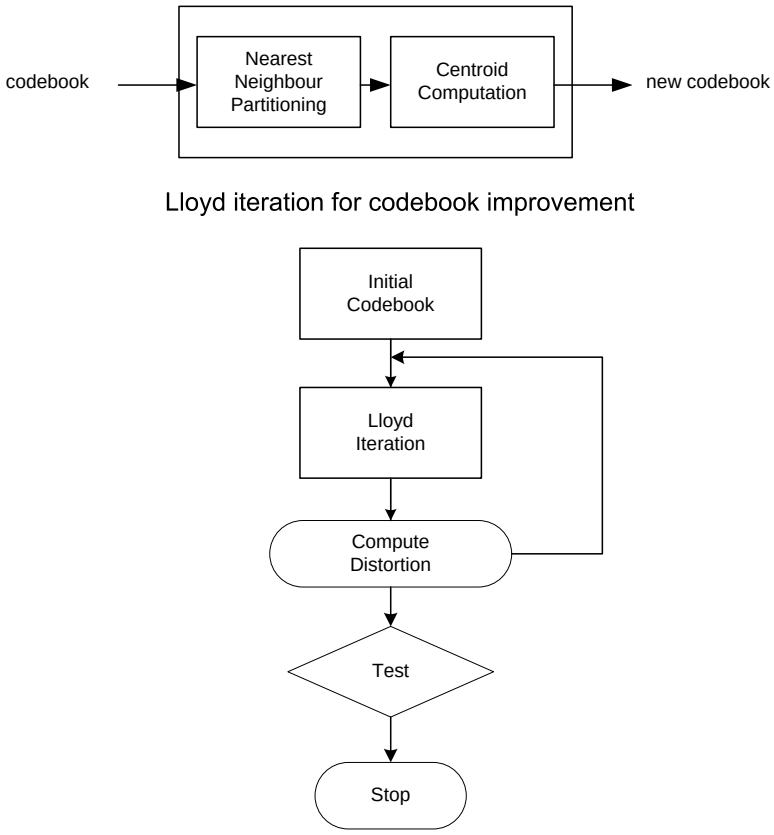

Figure 2.4: Flow chart of the Lloyd algorithm for quantizer design.

The distortion rate function [39] of a source is used to determine the minimum achievable average distortion for a given source-coder output rate. The distortion-rate function of a fixed rate optimal scalar quantizer [40] for large values of rate (R) is given as:

$$\delta(R) \approx \frac{1}{12}\left(\int f^{1/3}(x)dx\right)^3 2^{-2R}. \tag{2.9}$$

Entropy Constrained Scalar Quantization

Shannons work [2] also provides insight into lossless source coding. It showed that the allocation of equal number of bits for every region of a quantizer was suboptimal if the probability of occurrence of data over every region was unequal. The average number of bits being generated can be reduced by assigning shorter codewords to regions with higher probabilities, while encoding lesser probable regions with longer codewords. A quantizers

having binary codewords of varying lengths assigned to each regions is known as a variable rate quantizer. Scalar quantizes produce fixed rate codewords. The application of variable-length lossless coding (entropy coding) to the output of a scalar quantizer would produce variable length codewords and reduce the average number of bits being transmitted.

Entropy defines the number of bits on average required to describe the random variable and provides a limit on the best possible lossless encoding or compression achievable [41]. If the quantizer outputs are followed by entropy coding (lossless coding), the rate of the lossless codes would be equal to the entropy of the quantizer output and can be denoted as $H(Q)$. Naturally, minimizing both $H(Q)$ and D would be optimal. However, these quantities are inversely related. A scalar quantizer achieving the minimal D subject to an entropy constraint $H(Q) \leq R$ is called an entropy constrained scalar quantizer (ECSQ) [42]. Renyi [43] showed that a uniform scalar quantizer with infinitely small partitions of width Δ have the quantizer output entropy given by

$$H(q(X)) \approx h(X) - log\Delta, \tag{2.10}$$

where h(X) is the differential entropy [41] of the source variable X defined as

$$h(X) = -\int f(x) log f(x) dx \tag{2.11}$$

The works of Koshelev [40] and Zador [40] prove that when the rate is high, uniform quantizers were the optimal entropy constrained scalar quantizers for the application of variable rate encoders and that the operational rate-distortion function of a variable-length quantizer with a large rate is given as:

$$\delta(R) \approx \frac{1}{12} 2^{2h(X)} 2^{-2R}. \tag{2.12}$$

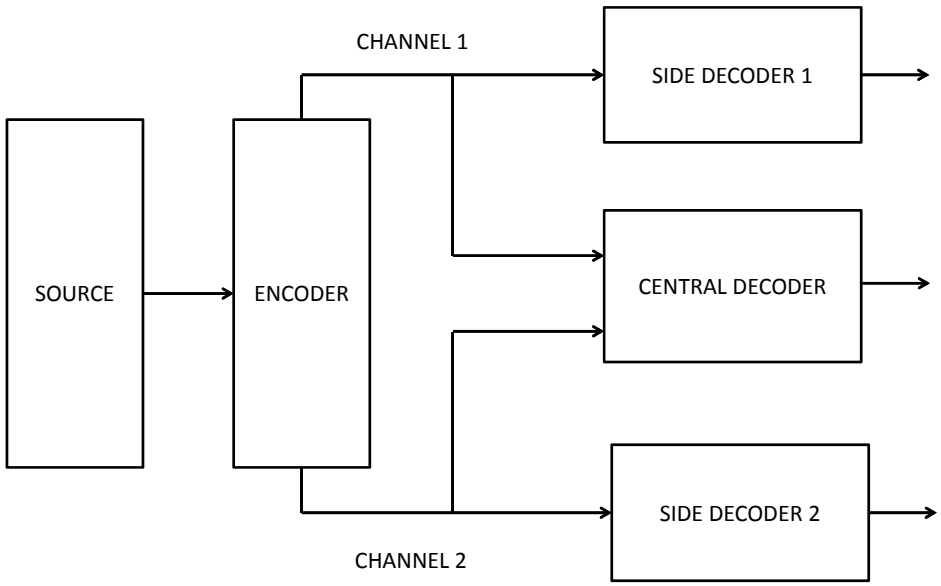

Figure 2.5: Multiple Description Coding Problem

2.2 Multiple Description Coding

If losses are inevitable, codewords that make all of the received data useful for reconstruction, irrespective of the order in which they are received, can be of great benefit. MDC creates such codewords.

MDC has its origination at Bell Laboratories in connection with the transmission of speech over the telephone network [12]. The speech from a call was split into two parts which were directed on two separate links or paths. Each component carried enough information to reproduce the call with a lowered voice quality. Under normal circumstances, both parts would be received and can be combined to attain the standard voice quality. On the other hand, the splitting of data allowed the compensation of one link outage by reducing the voice quality.

The MDC problem was formalized by Gersho, Witsenhausen, Wolf, Wyner, Ziv, and

Ozarow in an IEEE-Information Theory Workshop in September 1979 [44]. MDC with two descriptions can be described as follows (See fig. 2.5) . The encoder maps the source information into two description X_1 and X_2 with rates R_1 and R_2 bits respectively. Each descriptions is then communicated over two independent channels. The receiver has three decoders, a central decoder and two side decoders. The central decoder receives the descriptions sent over both the channels producing distortion D_0. The side decoders, on the other hand, only receive the descriptions sent over their respective channels, thus, inducing distortions D_1 and D_2 respectively.

The conflicting requirements to be met at the side and central decoders make the design of MDC a challenging problem. If each description is optimal for the input at its rate (R_1 or R_2), then taken together they cannot be optimal for the sum rate $R_1 + R_2$. That is, having two good descriptions at rates R_1 and R_2 which are similar to each other does not give any gain at the central decoder. On the contrary, a *good* description of the source at $R_1 + R_2$ bits, cannot be easily split into two descriptions which are individually good. The fundamental trade-off in MDC is that of producing individually good descriptions which are almost similar yet different enough to yield a gain at the central decoder.

2.3 Quantized Frame Expansion

Frames were first introduced in the work of Duffin and Schaeffer in 1952 [45]. In this thesis, quantized frames expansions are used as generalized MDC of the source.

2.3.1 Definition of Frames

In any Hilbert space, a vector $\Phi = \{\varphi_k\}_{k=1}^{M} \subset \Re^N$, is called a *frame* [30] if there exists $0 < A \leq B < \infty$ such that

$$A\|x\|^2 \leq \sum_{k=1}^{M} |\langle x, \varphi_k \rangle|^2 \leq B\|x\|^2. \tag{2.13}$$

A , B are called the *frame bounds* and x being any vector belonging to the Hilbert space. The lower bound in (2.13) is equivalent to requiring that Φ spans $\Re^N$, so a frame will always have $M \geq N$. The ratio $r = \frac{M}{N}$ is defined as the *redundancy* of the frame. Thus, for a frame Φ in $\Re^N$, the associated *frame operator F* is the linear operator from $\Re^N$ to $\Re^M$ defined as

$$y = (Fx)_k = \langle x, \varphi_k \rangle; \text{for } k = 1, 2, \ldots, M. \tag{2.14}$$

where the elements of y are the codewords or *coefficients* produces by the frame operator F

2.3.2 Reconstruction from Frames

The original signal x can be recovered from frame representations or coefficients y with the help of *Moore-Penrose generalized inverse or pseudoinverse* [46] of the frame operator F. The expression for the same is given by

$$F^{\mp} = \left(F^T F\right)^{-1} F^T, \tag{2.15}$$

where frame conditions ensure that (2.15) exists. Given a frame operator F and the frame coefficients y, the source can be reconstructed as

$$F^{\mp} y = F^{\mp}(Fx) = x \text{ for all } x \epsilon \Re^N. \tag{2.16}$$

The pseudo-inverse is precisely the transpose of the frame operator associated with the dual frame, that is,

$$F^{\mp} = \tilde{F}^*. \tag{2.17}$$

Reconstructing x with the pseudo-inverse is equivalent to using the frame expansion coefficients as weights in a linear combination of dual frame elements,

$$x = F^{\mp}(Fx) = \tilde{F}^*(Fx) = \sum_{i=1}^{M} \langle x, \varphi_i \rangle \tilde{\varphi}_i. \tag{2.18}$$

2.3.3 Quantization of Frame Coefficients

The frame coefficients y produced are analog in nature and would have to be quantized into discrete values $\hat{y}$. Each coefficient y_i for $i = 1 \cdots M$ is scalar quantized.

The process of quantization can be considered as the addition of noise to the original signal $y_i = \hat{y_i} + \eta_i$. Although, the quantization noise in this case is usually a deterministic function of the input, however, modeling the quantization noise stochastically leads to tractable analyses and useful results. It is assumed that,

- Each noise component η_i has zero mean and variance σ_i^2

$$E[\eta_i] = 0 \tag{2.19}$$

- The noise components are uncorrelated

$$E[\eta_i \eta_j] = \delta_{ij}\sigma^2 \text{ for all } i.j \tag{2.20}$$

Given that (2.19) and (2.20) are the only assumptions about the noise, the problem of finding a $\hat{x}$ that would minimize the error $\|F\hat{x} - \hat{y}\|_2$ is given by the the pseudo-inverse of F [46].

$$\hat{x} = F^{\mp}\hat{y} \tag{2.21}$$

By letting $\hat{y} = Fx + \eta$ in (2.21), we get

$$\hat{x} = F^{\mp}\hat{y} = F^{\mp}(Fx + \eta) = \sum_{i=1}^{M} \left(\langle x, \varphi_i \rangle + \eta_i\right) \tilde{\varphi}_i. \tag{2.22}$$

The resulting reconstruction error can be calculated as

$$x - \hat{x} = \sum_{i=1}^{M} \langle x, \varphi_i \rangle \tilde{\varphi}_i - \sum_{i=1}^{M} \left(\langle x, \varphi_i \rangle + \eta_i\right) \tilde{\varphi}_i = -\sum_{i=1}^{M} \eta_i \tilde{\varphi}_i. \tag{2.23}$$

The MSE for the reconstruction process can be computed as

$$MSE = \frac{1}{N}E\|x - \hat{x}\|^2 = \frac{1}{N}E\left\|-\sum_{i=1}^{M}\eta_i\tilde{\varphi}_i\right\|^2 = \frac{1}{N}E\left[\sum_{i=1}^{M}\sum_{j=1}^{M}\eta_i\eta_j\tilde{\varphi}_i\tilde{\varphi}_j\right]. \tag{2.24}$$

$$= \frac{1}{N}\sum_{i=1}^{M}\sum_{j=1}^{M}\delta_{ij}\sigma^2\tilde{\varphi}_i\tilde{\varphi}_j = \frac{1}{N}\sigma^2\sum_{i=1}^{M}\|\tilde{\varphi}_i\|^2. \tag{2.25}$$

2.3.4 Effects of Erasures

It is possible for the coefficients to be lost during transmission. Let the erased components of the quantized frame coefficients, $\hat{y}$, be z and the index of the set of components lost be E, that is, $\{\hat{y}_k\}_{k\in E}$ are the lost frame coefficients. At the receiver, the decoder can perceive the received coefficients to have been generated using a frame $\Phi_E = \{\phi_k\}_{k\notin E}$ assuming that Φ_E is a frame. In effect, the frame operator becomes $F_E = L_E F$, where the L_E captures the losses occurred. L_E is the $(M - e) \times M$ matrix obtained from an $M \times M$ matrix by deleting the rows corresponding to the elements of E.

If the number of erasures that occur are more than $M - N$, the remaining coefficients are too few to span the original space. However, if the number of erasures is less than $M - N$, the MSE can be calculated as [30]

$$MSE_e = \left(1 + \sum_{i=1}^{e}\frac{\mu_i}{M - N\mu_i}\right)MSE_0, \tag{2.26}$$

where MSE_0 is given by (2.25) and $\{\mu_i\}_{i=1}^{e}$ are the eigenvalues of $\varphi^*\varphi$. If the lost coefficients are orthogonal pairs, then (2.26) becomes

$$MSE_e = \left(1 + \frac{e}{M - N}\right)MSE_0. \tag{2.27}$$

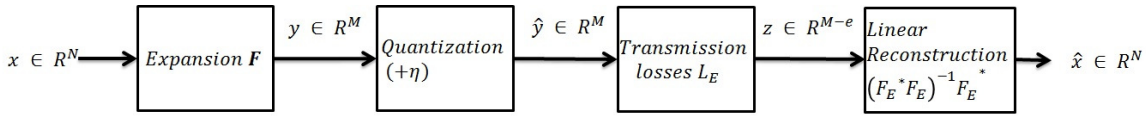

Figure 2.6: Transmission using Frames

2.3.5 Harmonic Tight Frames

Harmonic tight frames [30] are a class of unit norm tight frames [1] in $\mathbb{R}^N$. One of their most useful property is that any subset of N vectors from a harmonic frame still spans the space. The frame operator for such frames can be expressed as

$$f_{k+1} = \sqrt{\frac{2}{N}} \left[sin\frac{\pi k}{M}, cos\frac{\pi k}{M}, sin\frac{3\pi k}{M}, \cdots, sin\frac{\pi(N-1)k}{M}, cos\frac{\pi(N-1)k}{M} \right]^T \quad (2.28)$$

ff N is even, and,

$$f_{k+1} = \sqrt{\frac{2}{N}} \left[\frac{1}{\sqrt{2}}, sin\frac{2\pi k}{M}, cos\frac{2\pi k}{M}, sin\frac{4\pi k}{M}, \cdots, sin\frac{\pi(N-1)k}{M}, cos\frac{\pi(N-1)k}{M} \right]^T \quad (2.29)$$

if N is odd.

Let $\Phi = \{\varphi_k\}_{k=1}^M \subset \Re^N$ be a harmonic frame. Then any subset of N or more vectors from Φ would form a frame,$i.e.$,Φ_{M-N} forms a frame [30]. This property of harmonic frames ensures that (2.18) can be implemented for data reconstruction as long as the number of coefficients received at the decoder are greater than or equal to the the dimension of the original signal space.

[1] If the frame bounds 2.13 can be taken to be equal, then a frame is called a tight frame [30]

Chapter 3

An Approach To Adaptive Joint Source-Channel Coding For Cognitive Radio

Multimedia applications are a mixture of various source signals which include data, text, audio, image and video. Real-time multimedia content require significant bandwidth. The limitation of the available bandwidth is considered to be on the major bottlenecks of high-quality multimedia wireless services. Cognitive radios allow us to access the under utilized wireless frequency spectrum, thereby, increasing the bandwidth available. Given the challenges discussed in Sec. 1.1, this thesis focusses on the reliable real time transmission of multimedia in a cognitive radio environment.

In this chapter, a new approach to adaptive JSCC for SU transmission in a cognitive radio network is developed. This thesis considers the coding problem of a SU which transmits multimedia signal in a cognitive radio environment with N PUs. Each PU is assumed to have a single licensed channels which is accessed by the SU intermittently in a random manner. The SU transmitter and receiver periodically sense the cognitive radio environment to detect vacant PU channels for transmission of its data. The proposed JSCC scheme adaptively encodes the data to be transmitted over one or more vacant PU channels. The

proposed JSCC scheme takes the probability of packet loss due to PU arrivals in optimally encoding the source signal. Figure 3.1 depicts the problem set-up being considered in the thesis.

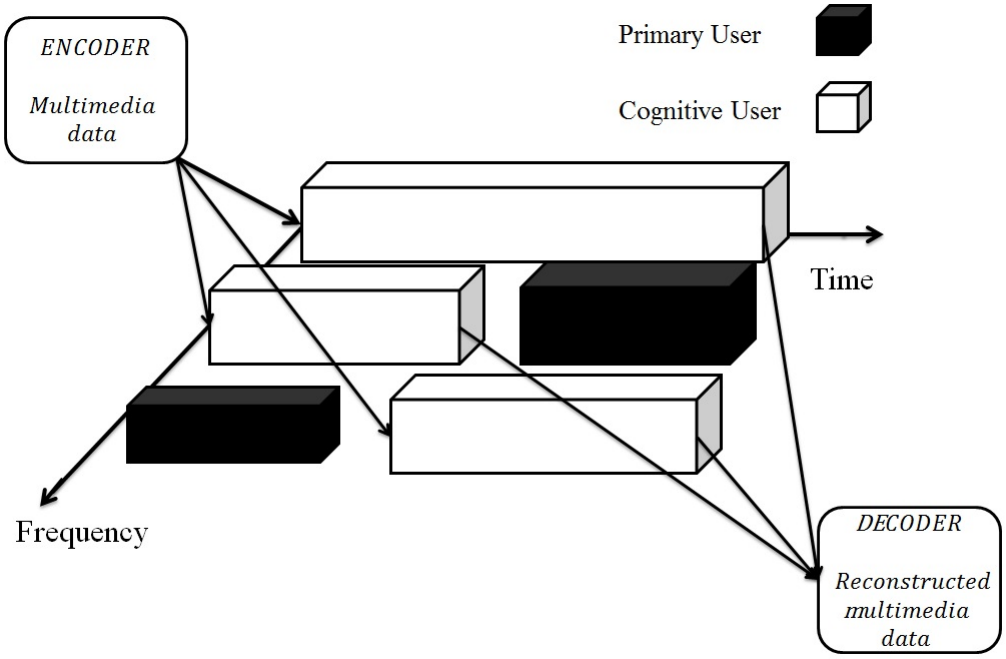

Figure 3.1: SU multimedia transmission over cognitive radio.

3.1 System Model

3.1.1 PU Model

Let the number of PUs in the cognitive radio environment be N, each with a single licensed channel. The number of channels available to the SU at any time instant cannot exceed N. In this section, a model used to represent the random traffic arrivals on a PU channel are described. A model for the PU channel is then presented, upon which the JSCC code design is to be based.

PU Arrival Model

The measurement studies in [47] and [48] show that the PU arrivals in a cognitive radio environment can be well modelled by a Poisson process. Poisson processes also allow us to capture the dynamic nature of a cognitive radio network. In this thesis, PU arrivals are modelled as a Poisson process with the arrival rate of λ. We assume that the arrival process during every SU transmission is stationary in nature. The Poisson distribution parameter λ can therefore, be calculated using maximum likelihood estimation as

$$\begin{aligned} \hat{\lambda} &= \frac{1}{\bar{x}}, \\ \text{where,} \quad \bar{x} &= \sum_{i=i}^{n} x_i \end{aligned} \tag{3.1}$$

and $x = (x_1, \cdots, x_n)$ are the value observation seen during n-sized window for observations [49].

PU Channel Modelling

The N PU channels would all exhibit different channel characteristics, that is, it is not necessary the properties of each PU channel be the same. Let the PU arrival rate, packet loss probability (due to fading, etc.) and the capacity of the PU channel i be λ_i, α_i and C_i respectively. The arrival rate, the packet loss probability and the channel capacity are collectively taken as a vector CP_i, which defines every PU channel i in the cognitive system.

$$CP_i = \begin{bmatrix} \lambda_i & \alpha_i & C_i \end{bmatrix}^T \tag{3.2}$$

The channel loss probability can be estimated using either pilot signals or by using methods described in [50].

3.1.2 SU Model

At any given time, the network is assumed to consist to S SU pairs of source and destination nodes. The availability of a channel j for a SU s can be indicated as $a(s, j)$, wherein

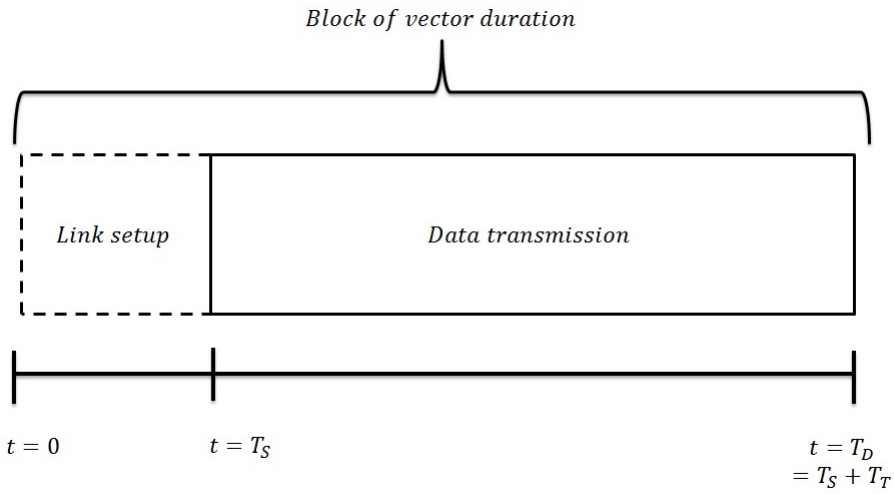

Figure 3.2: BOV duration phases.

$a(s, j) = 1$ indicates the availability of channel j and $a(s, j) = 0$ indicates otherwise. When the transmitter and receiver have common channels available, they are able to communicate on those channels. If the transmitter and the destination sense different channels being available, the communication becomes infeasible.

Block of Vector Structure

Data transmission by a SU occurs on a block by block basis. The arrival of a new block of source vectors at the SU indicates the requirement for transmission to the SU source. It is assumed that a block of vectors (BOV) should be transmitted within time T_D. SU transmission of BOV consists of two phases as shown in fig. 3.2. The sensing of the vacant PU channels along with the determining the required redundancy is considered to be the *link set-up* phase while the transmission of the BOV occurs during the *data transmission* phase. Let T_S and T_T denote the time for link set-up and data transmission.

$$T_S + T_T \leq T_D \tag{3.3}$$

Communication Protocol

The following protocol is considered for the SU communications in the cognitive radio network [51]. The BOV duration can be seen as four major time periods, wherein the link set-up can be further divided into sensing, access and optimization periods while the transmission period, as the name indicates, constitutes the transmission time.

- *Sensing period* : Each SU (source and destination) senses the spectrum and determines the available channels. It chooses the available channels as its working channels. For a transmitter, the working channels are for transmitting the data, while for a receiver the working channels are for listening.

- *Access period*: The source sends a request-to-send (RTS) on the channels it detects as available. When the destination node receives a RTS on any of its working channels, it sends back a clear-to-send (CTS), thereby establishing the connection between the source and the destination pair on that particular channel.

- *Optimization period*: Based on the knowledge of the channels available for transmission and the channel conditions pertaining to each of these available channels, the source and destination independently calculate the redundancy required based on the optimization algorithm presented in this thesis. Since the algorithm used by the transmitter and the receiver are identical, they produce the same channel estimates, thereby eliminating the communication overhead required to establish the same channel state information at the transmitter and the receiver

- *Transmission period*: The transmission between the source node and the destination node takes place.

SU Operation

The functioning of any SU can be divided among two major tasks:

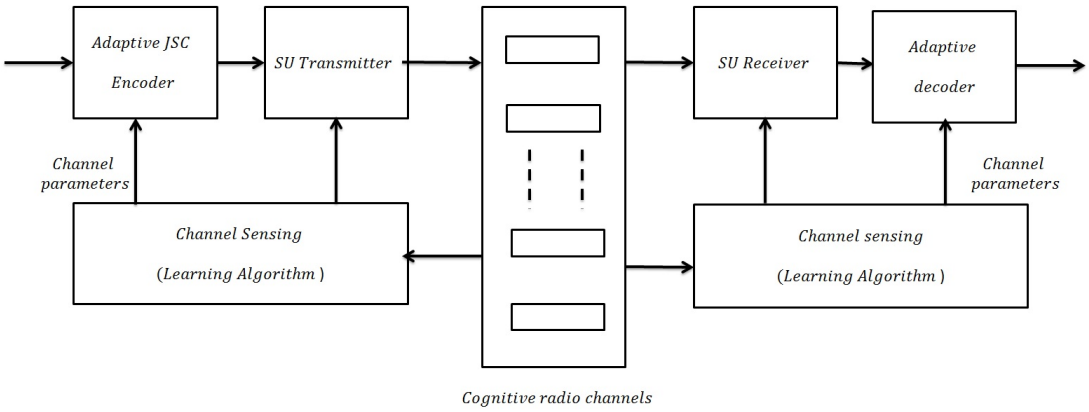

Figure 3.3: SU operation.

1. *Estimation of channel parameter* : We assume that each SU has an underlying learning layer as shown in fig. 3.3. Although not a part of the encoder used for data transmission, this layer is responsible for the estimation of the PU arrival rates using (3.1) and for the estimation of the channel loss probabilities. At the beginning of each SU communication frame, the sensing and access period results are utilized by this layer for estimating the channel parameters CP_i. The results so obtained are passed to SU encoder used for data transmission.

2. *JSCC using adaptive MDC* :The channel parameters estimated by the learning layer are passed to the encoder optimization algorithm. From a SU's perspective, the available channels appear as a multiple access channel system with different channel parameters. During a transmission slot, if a channel i is taken back by a PU at time t_k, then all the packets transmitted on channel i after time t_k are considered to be lost.

3.2 Problem Description

The source is taken to a be stationary random process $\underline{X} \in \mathbb{R}^K$ generated at the rate of R samples per unit time. During a transmission period, n source vectors are transmitted as shown in fig. 3.4. We assume the mean of the source vectors is zero and that the variance

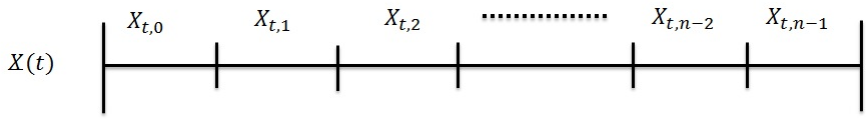

Figure 3.4: BOV of the source.

of the source vector is known.

$$\begin{aligned} E[X_{t,j}] &= 0 \\ E[X_{t,j}^2] &= \sigma_j^2. \end{aligned} \tag{3.4}$$

where t denotes the transmission time and $j = 0, \cdots, n-1$. Let the bit available per sample be r_S. The time required for generating $\underline{X}(t)$ is given by

$$T_{Gen} = \frac{nK}{R}, \tag{3.5}$$

and the total bit budget available is given by

$$B_t = nKr_S. \tag{3.6}$$

As shown in fig. 3.5, each vector $\underline{X}_{t,j}$ is expanded into $N_{t,j} \geq K$ coefficients (descriptions) using frame expansion.

$$\underline{Y}_{t,j} = F\underline{X}_{t,j} \tag{3.7}$$

where F is the frame operator matrix of dimension $N_{t,j} \times K$ and $\underline{Y}_{t,j} \in \mathbb{R}^{N_{t,j}}$ are the frame coefficients. We assume that the maximum delay allowable between the generation of these nK samples and its reception at the decoder should be equivalent to the time needed for

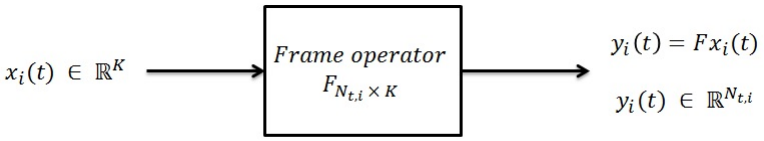

Figure 3.5: Frame expansion operation.

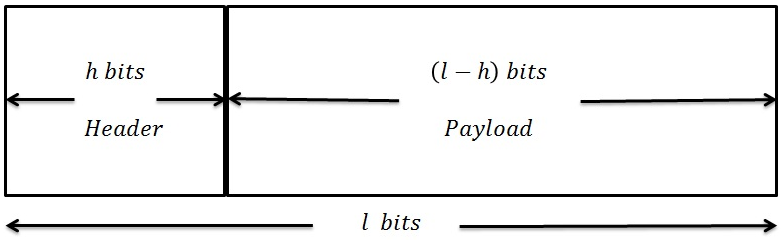

Figure 3.6: Packet structure.

the generation of these samples.

$$T_D = T_{Gen} = \frac{nK}{R} \tag{3.8}$$

3.2.1 Packet Structure

The packets being transmitted are of equal length [1], each being l bits long. The packet consists of two parts, the header and the payload, as shown in fig. 3.6. Let the header be h bits long. Hence, each packet carries a payload of $(l - h)$ bits. The maximum number of packets (L_t^{max}) required for the transmission of B_t bits is given by

$$L_t^{max} = \frac{B_t}{l - h} = \frac{nKr_s}{l - h}. \tag{3.9}$$

Let the channel capacity of each PU channel in the cognitive radio environment be C bits per unit time.The time required for the transmission of a packet on a channel is given as

$$T_p = l/C \tag{3.10}$$

The minimum number of channels (M_t^{min}) required for the transmission of the L_t packets is given by

[1] In [52], it was observed that the fixed length packet sizes achieve higher throughput efficiency when compared to exponentially distributed packet sizes for cognitive radio networks.

$$M_t^{min} = \frac{L_t^{max}}{T_T/T_p}$$

where, (3.11)

$$T_T = \frac{nK}{R} - T_S.$$

Let the total number of vacant channels at time t be β_t. If $\beta_t > M_t^{min}$ then channels are selected with respect to the PU arrival rates. The channel with the lower arrival rate are given precedence over the channel with higher PU arrival rate. Otherwise, all the available channels are used irrespective of the PU arrival rate. The number of channels used for transmission is given by

$$M_t = \begin{cases} M_t^{min} & M_t^{min} < \beta_t \\ \beta_t & \text{otherwise,} \end{cases} \tag{3.12}$$

where M_t is an ordered vector of channel indices (based on PU arrival rate) being used for transmission at time t. The actual number of packets then transmitted during each time t is given by

$$L_t = \begin{cases} L_t^{max} & M_t = M_t^{min} \\ \frac{T_T}{T_p} M_t & M_t \neq M_t^{min} \end{cases} \tag{3.13}$$

It is assumed that the L_t packets are distributed among the M_t channels. Each channel, therefore, carries L_t/M_t packets as depicted in fig. 3.7. If $L_t < L_t^{max}$, the total bit budget available then becomes $B_t = L_t \times (l - h)$.

Each source vector is described using frame coefficients $\underline{Y}_{t,j} \in \mathbb{R}^{N_{t,j}}$. The equal distribution of each of the generated coefficients among the L_t packets would ensure that every packet is equally important and has equal amounts of information. As shown in fig. 3.8, the equal distribution of the coefficients among L_t packets results in each packet carrying $[N_{t,j}/L_t]$ coefficients of the source vector $\underline{X}_{t,j}$,for $j = 0, \cdots, n-1$.

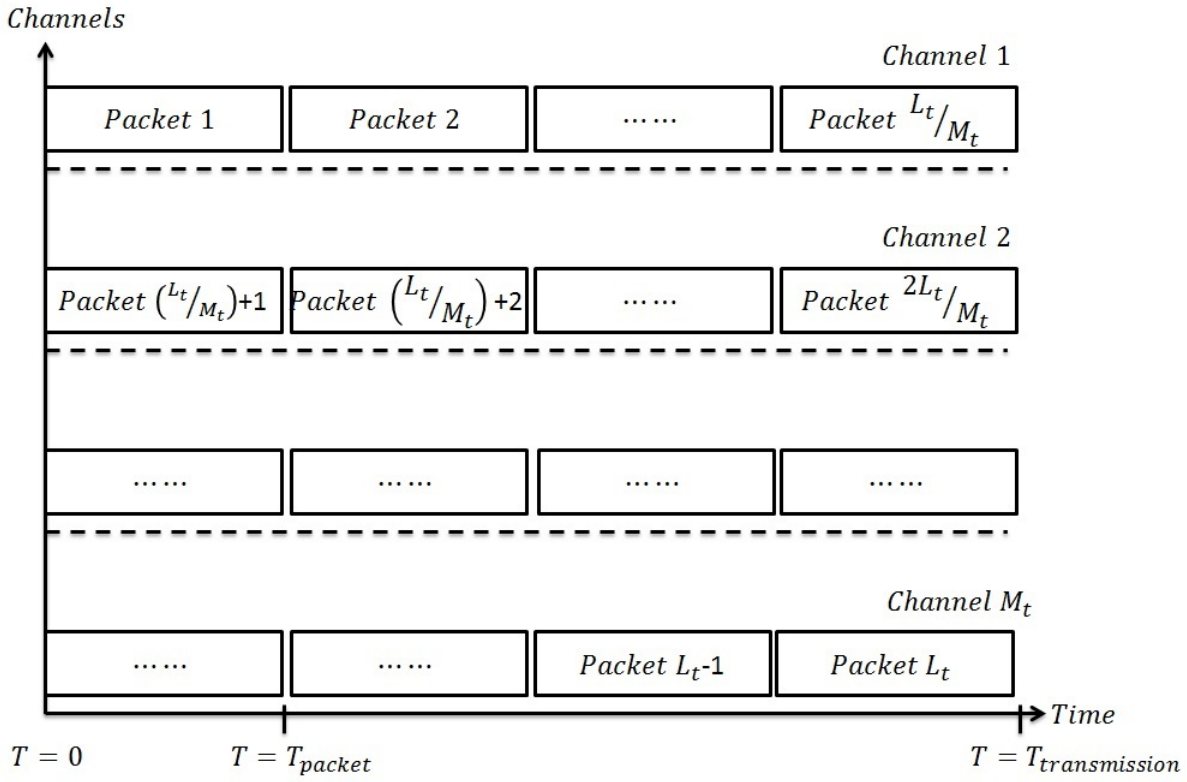

Figure 3.7: Packet distribution over M_t channels.

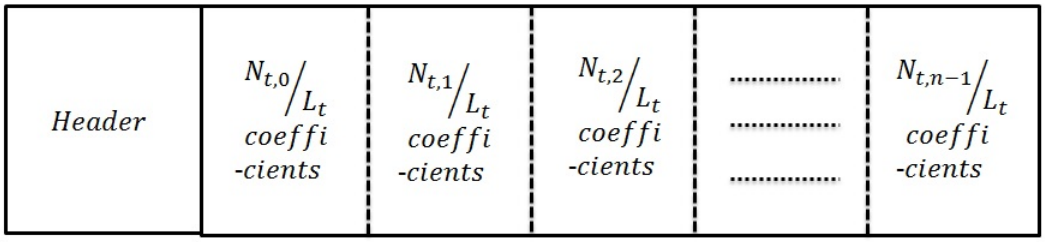

Figure 3.8: Coefficient distribution among packets.

3.2.2 Packet Loss Probability

Let the PU arrival on channel i be denoted as λ_i. Thus, the inter-arrival times of the PU traffic would be exponentially distributed with the mean arrival time of $\frac{1}{\lambda_i}$. Let the packet loss probability on each channel be α_i, the time available to a SU transmission on channel i before a PU arrival occurs on that channel be T_i and the number of packets received by the

decoder on channel i be η_i, where $\eta_i = 0, \cdots, L_t/M_t$ and $i = 1, \cdots, M_t$. The event that exactly η_i packets are received on channel i is equivalent to the condition that the channel is available until exactly η_i packets are completely transmitted. The amount of time required for the complete transmission of η_i packets is given by $\eta_i T_p$. If a PU arrival occurs after $(\eta_i + 1)T_p$, then $\eta_i + 1$ packets would have been received. For the reception of exactly η_i packets, the PU traffic should arrive after $\eta_i T_p$ but before $(\eta_i + 1)T_p$. Therefore, the probability of receiving η_i packets is equal to the probability of T_i being greater than or equal to $\eta_i T_p$ but less than $(\eta_i + 1)T_p$. Similarly, the probability of receiving all the packets on a channel is equal to the probability that the PU arrival occurs after T_T. Hence, it follows that

$$P_{packets}(\eta_i) = \begin{cases} P[\eta_i T_p \leq T_i < (\eta_i + 1)T_p] & \eta_i < \frac{L_t}{M_t} \\ P[T_i \leq T_T] & \eta_i = \frac{L_t}{M_t} \end{cases}. \tag{3.14}$$

Since the inter-arrival times of the PU on the i^{th} channel is assumed to exponentially distributed, the pdf of T_p is given by

$$f_{T_i}(t) = \lambda_i e^{(-\lambda_i t)} \text{ for } t \geq 0. \tag{3.15}$$

Therefore, the probability of the decoder receiving exactly η_i packets on the i^{th} channel is given by

$$P_{packets}(\eta_i) = (1 - \alpha_i) \int_{\eta_i T_p}^{x} \lambda_i e^{(-\lambda_i t)} dt \tag{3.16}$$

where $\eta_i = 0, \cdots, (L_t/M_t)$ and,

$$x = \begin{cases} (\eta_i + 1)T_p & (\eta_i + 1)T_p < T_T \\ \infty & (\eta_i + 1)T_p \geq T_T \end{cases}. \tag{3.17}$$

The total number of packets received by the decoder on all M_t channels is given by

$$\bar{\eta} = \sum_{i=1}^{M_t} \eta_i. \tag{3.18}$$

The total probability of receiving $\bar{\eta} = 0, \cdots, L_t$ packets over the M_t channels is given by the convolution of the probabilities across each channel,that is,

$$P_{total}(\bar{\eta}) = \bigotimes_{i=1}^{M_t} P_{packets}(\eta_i). \tag{3.19}$$

The probability that $c_j(t)$ frame coefficients of the j^{th} source vector is received at the decoder is given by

$$P_{tj}\left(c_j(t) = w\frac{N_{t,j}}{L_t}\right) = P_{total}(\bar{\eta} = x). \tag{3.20}$$

where, $c_j(t) \in \left\{0, \frac{N_{t,j}}{L_t}, \cdots, N_{t,j}\right\}$, $j = 0, \cdots, n-1$ and $w = 0, \cdots, L_t$

3.2.3 Average Distortion

The application of harmonic tight frames allows any subset of K coefficients to still function as a frame. In our encoder design, we assume that the decoder can successfully decode only if the received coefficients form a frame. Thus, if the decoder receives anything less than K coefficients, the source is optimally estimated based on prior information only. It is well known that under the MSE distortion measure, the optimal estimate is the mean value of the source and the resulting distortion is the variance of the source.

On the other hand, the reception of K or more coefficients allows the successful reconstruction of the transmitted samples. From (2.27) it follows that the MSE for a source vector j with e erasures at time instance t can be expressed as

$$\begin{aligned} D_{tj}(e) &= \frac{1}{K} E\left\{\|\underline{X}_{TJ} - \underline{\hat{X}}_{TJ}\|^2 | T = t; \mathbb{E}_t = e; J = j\right\} \\ &= \begin{cases} \sigma_j^2 & e > N_{t,j} - K \\ \left(1 + \frac{e}{N_{t,j}-K}\right)\left(\frac{K}{N_{t,j}}\right) D_q(b_{t,j}) & e \leq N_{t,j} - K \end{cases}. \end{aligned} \tag{3.21}$$

where $D_q(b_{t,j})$ is distortion of the quantizer for the rate of $b_{t,j}$ bits. The MSE for a BOV is

given by

$$\begin{aligned} D_{BOV} &= \frac{1}{nK} E\left\{ \|\underline{X}_T - \underline{\hat{X}}_T\|^2 | T = t \right\} \\ &= \frac{1}{nK} \sum_{j=0}^{n-1} E\left\{ \|\underline{X}_{TJ} - \underline{\hat{X}}_{TJ}\|^2 | T = t; J = j \right\} \\ &= \frac{1}{nK} \sum_{j=0}^{n-1} \sum_{e \in \mathbb{E}_t} E\left\{ \|\underline{X}_{TJ} - \underline{\hat{X}}_{TJ}\|^2 | T = t; J = j; \mathbb{E}_t = e \right\} \\ &= \frac{1}{n} \sum_{j=0}^{n-1} \sum_{e \in \mathbb{E}_t} P_{tj}(N_{t,j} - e) D_{tj}(e) \end{aligned} \tag{3.22}$$

where, $\mathbb{E}_t = \left\{ 0, \frac{N_{t,j}}{L_t}, \cdots, N_{t,j} \right\}$. Therefore the MSE of the entire source is given by

$$\begin{aligned} D_F &= \frac{1}{nK} E\left\{ \|\underline{X} - \underline{\hat{X}}\|^2 \right\} \\ &= \lim_{T \to \infty} \frac{1}{T} \frac{1}{nK} \sum_{t=1}^{T} E\left\{ \|\underline{X}_T - \underline{\hat{X}}_T\|^2 | T = t \right\} \\ &= \lim_{T \to \infty} \frac{1}{T} \frac{1}{nK} \sum_{t=1}^{T} \sum_{j=0}^{n-1} E\left\{ \|\underline{X}_{TJ} - \underline{\hat{X}}_{TJ}\|^2 | T = t; J = j \right\} \\ &= \lim_{T \to \infty} \frac{1}{T} \frac{1}{nK} \sum_{t=1}^{T} \sum_{j=0}^{n-1} \sum_{e \in \mathbb{E}_t} E\left\{ \|\underline{X}_{TJ} - \underline{\hat{X}}_{TJ}\|^2 | T = t; J = j; \mathbb{E}_t = e \right\} \\ &= \lim_{T \to \infty} \frac{1}{T} \frac{1}{n} \sum_{t=1}^{T} \sum_{j=0}^{n-1} \sum_{e \in \mathbb{E}_t} P_{tj}(N_{t,j} - e) D_{tj}(e) \end{aligned} \tag{3.23}$$

3.2.4 Rate-Expansion Trade-off

Given $\lambda_1, \cdots, \lambda_{M_t}$, large frame expansions $N_{t,j}$ will reduce the probability of losing coefficient. However, since the channel bit rate is fixed, increasing the expansion $N_{t,j}$ will decrease the bit available for each coefficient resulting in increased quantization error. This would in turn result in a higher distortion. On the contrary, using smaller frame expansions $N_{t,j}$ would induce smaller quantization error, but would cause the probability of losing packets to increase. This again would result in a large error. The proposed JSCC finds the unique set of $\{N_{t,j}\}$, for $j = 0, \cdots, n-1$ which minimizes the MSE given by (3.22)

3.2.5 Code Optimization

The channels availability along with the knowledge of the channel conditions CP_i makes it possible to calculate the MSE for a given expansion factor $N_{t,j}$. From (2.13), we know that the frame operator should atleast be a $K \times K$ matrix. Each packet strictly carries at the most K coefficients for $\underline{X}_{t,j}$, $j = 0, \cdots, n-1$. Hence, the maximum allowable expansion is given by

$$K \times L_t. \tag{3.24}$$

The optimization algorithm uses (3.22) to calculate the conditional MSE for the different expansions possible, $K \leq N_{t,j} \leq K \times L_t$ for each source vector $\underline{X}_{t,j}$, $j = 0, \cdots, n-1$. The algorithm then selects the expansion factor yielding the minimal conditional MSE for each source vector, thereby, resulting in the selection of the expansion factors with the minimal total MSE. The algorithm is used to optimally adapt the JSCC to varying channel conditions at the start of each time slot.

3.3 Code Design for Gaussian Sources

In this section, we discuss the application of the developed adaptive JSCC algorithm to transmitting a Gaussian source. The developed JSCC algorithm is applied to a sequence of independent and identically distributed(*iid*) Gaussian function with mean zero and variance σ^2. Next, the analysis is extended to Gaussian sources with unequal variance where we develop an algorithm to incorporate bit allocation for the proposed JSCC.

3.3.1 Identically Distributed Gaussian Sources

Since the source sample are *iid*, the bit allocation and the optimal expansion for all source vectors will be the same, *i.e.*, the bit allocation for each quantizer must be the same. There-

fore, the bit allocated to each expansion coefficient of the source vector is given by

$$b_{t,j} = \frac{r_s K}{N_{t,j}} \text{ where } j = 1, \cdots, n. \tag{3.25}$$

Also,

$$b_{t,j} = b_{t,k} \text{ for any } j, k. \tag{3.26}$$

3.3.2 Non-identically Distributed Gaussian Sources

We consider the transmission of q Gaussian sources with different variances σ_i^2 for $j = 1, \cdots, q$. Let n denote the number of source vectors taken from each Gaussian source of variance σ_i^2. The BOV is formed as shown in fig. 3.9. The total bits available is given by

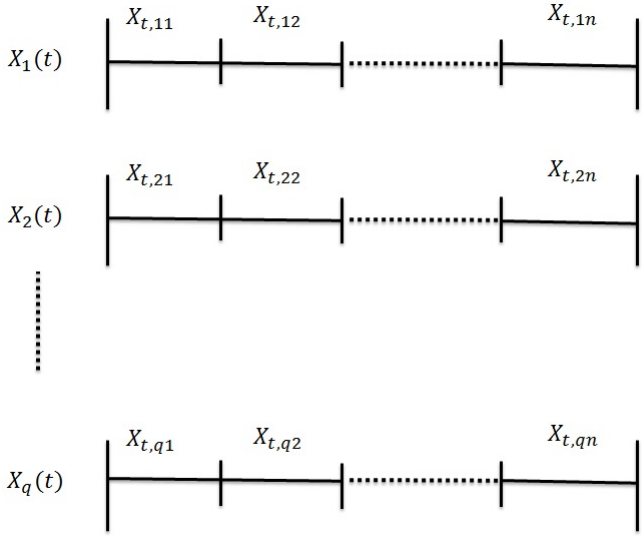

Figure 3.9: BOV for Gaussian sources with different variances.

$$B_t = nqKr_s \tag{3.27}$$

Unlike with *iid* sources, the total bit budget of B_t bit per BOV must be optimally allocated between the q sources in order to minimize (3.22). The problem of bit allocation is to determine optimal bit allocations $b_{t,jk}$ that would minimize the total MSE given $B_t = \sum_{j=1}^{q} \sum_{k=1}^{n} b_{t,jk}$. In this section, we develop a bit allocation algorithm for this problem,

which can be incorporated into the adaptive JSCC algorithm described in Sec. 3.2.

Bit Allocation Algorithm

[34] assumes high rate distortion approximation, and provides the solution for optimally allocating bits among identically distributed random variables as

$$b_{t,j} = \bar{b} + \frac{1}{2} log_2 \frac{\sigma_j^2}{\rho^2} \tag{3.28}$$

where, $b_{t,j}$ is the bit allocated to the source with variance σ_j^2,

$$\rho^2 = \left(\prod_{i=1}^{n} \sigma_i^2 \right)^{\frac{1}{n}} \tag{3.29}$$

ρ is the geometric mean of all variances and $\bar{b} = \frac{B}{n}$ is the average number of bits per group. This scheme, however, focusses on minimizing the overall distortion due to the quantizer implementation but does not focus on the reduction of the total distortion shown in (3.22). Moreover, the optimal bit allocation so achieved is not guaranteed to be integer valued as would be the requirement for fixed rate quantizers. Hence, (3.28) cannot be used in the JSCC implementation.

The problem of finding optimal bit allocations that would minimize (3.22) over all choices of $b_{t,jk}$, for $j = 1, \cdots, q$ and $k = 1, \cdots, n$ would be combinatorial in nature. It would be impractical to find all the combinations possible for bit allocation in order to determine the optimal bit allocation that would minimize the total MSE. Using the idea of greedy bit allocation algorithm presented in [34], this thesis presents a similar algorithm that tries to minimize (3.22) while attempting to find a nearly optimal bit allocation that can be incorporated into the proposed JSCC. At each step of the algorithm, Δb bits are allocated to the quantizer that would cause the maximum reduction in the overall distortion. Fig. 3.10 illustrates the flow chart for the algorithm. The distortion produced at each source is calculated by (3.22). The algorithm searches for the source producing the maximum reduction in distortion at each iteration and allocates the bit to the quantizer of this source.

The process is re-iterated until all the available bits are allocated. The algorithm is short sighted in nature and prefers to attain the maximum immediate reduction possible in the distortion disregarding the long-term or global effect of the decision.

The detail on the application of the proposed bit allocation algorithm is show in in table 3.1. We define the bit quantity being assigned at each iteration as Δb, allowing Δb to be integer for fixed rate quantizers and fractional for entropy coded quantizers. [53] shows that the distortion given by (2.12) exceeds σ^2 for rates below 0.255 bits. Therefore, the range for Δb is taken to be $0.255 \leq \Delta b \leq 1$

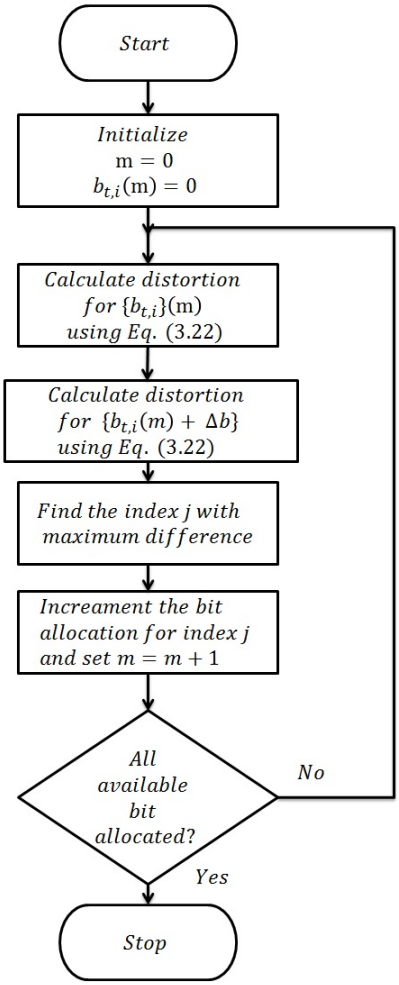

Figure 3.10: Flowchart for proposed bit allocation algorithm.

Table 3.1: Proposed Bit Allocation Algorithm

Step number	**Procedure**
Step 1	Initialize the bit allocations for all groups and the tracker m to zero. That is, $b_{t,i}(m) = 0$ for all $i = 0, \cdots, n-1$ and $m = 0$.
Step 2	Set the initial demands $d_i(0) = W_i(0)$ where $W_i(b)$ is calculated using 3.22 for $b_{t,i}(m) = 0$
Step 3	Find the demands $d_{new,i}(m)$ for $b_{t,i}(m) + \Delta b$
Step 4	Find the index with the maximum difference between $d_{new,i}(m)$ and $d_i(m)$ for the current value of m and assign it as q.
Step 5	Increment the bit allocation for group $i = q$ by the small fraction Δb. Therefore $b_{t,q}(m+1) = b_{t,q}(m) + \Delta b$. The bit allocations for the other indices remains unchanged, that is, $b_{t,i}(m+1) = b_{t,i}(m)$ for $i \neq q$.
Step 6	Find the new demands $d_i(m+1) = W_i(m+1)$ with $b_{t,i}(m+1)$.
Step 7	Set $B = B - \Delta b$ and $m = m + 1$.
Step 8	If $B > 0$ go to *Step 3*. Else stop.

3.4 Code Design for Images

This section discusses the application of the proposed JSCC algorithm to an image transmission. Firstly, the proposed JSCC is applied to directly to an image being transmitted by the SU user. In the latter half of the section, we study the application of the proposed JSCC to the transmission of a *transform coded* [34] image.

3.4.1 Direct Coding for Pixels of an Image

In this section, we consider the transmission of image pixel directly. As each pixel of the image is equally important, the transmission of the image pixels in their raw form can be treated as the transmission of *iid* Gaussian source, wherein each source vector is equally important. The image pixels can be frame expanded using the proposed JSCC algorithm and transmitted over the cognitive radio environment with equal bit allocation.

3.4.2 Coding for Transform Coefficients of an Image

Correlation is defined at the degree to which two or more quantities are linearly associated. When a source is strongly correlated, that is, there are linear dependencies between the source components, the application of quantization to each component separately would be an inefficient way of encoding the data if there are limitations on the bit available. Transform coding [34] allows a suitable linear transformation of an m dimensional vector X, into another a m dimensional vector Y, such that elements of the transformed vector Y or *transformed coefficients* are less correlated. Furthermore, transform coding might allow the concentration of the information to only a few transformed coefficients, thereby, *compacting* the source vector X. Thus, with the limitation on the bits available, transform coding allows the scope for discarding lesser important coefficient. Fig. 3.11 adapted from [34] shows the process of transform coding where T indicates the process of transform coding, Q_i represents the scalar quantizer adapted to transform coefficient Y_i and T^{-1} represents the inverse of transform coding. The transform coefficients, in general, may have different variances. Therefore, each quantizer being implemented would require different bit allocations. The algorithms described in sec. 3.3.2 are used for allocating bits among the distinct quantizers.

The application of transform coding allows the linear transformation of an image into transform coefficients reducing the correlation between the pixels of the image. Discrete Cosine Transform (DCT) is considered in this thesis for the transform coding of images.

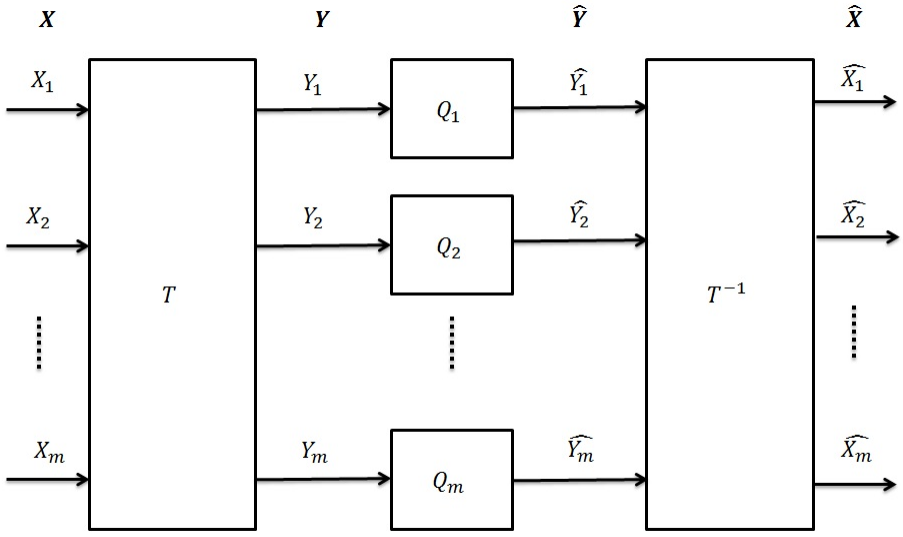

Figure 3.11: Transform coding.

DCT [54] is an orthogonal transform and produces a real transformed vector if the input vector is real in nature. DCT can be specified as a $m \times m$ matrix, where the ij^{th} element of the matrix can be represented by

$$t_{ij} = \begin{cases} \sqrt{\frac{2}{m}} \cos\left(\frac{\pi}{m} i \left(j + \frac{1}{2}\right)\right) & i = 1, 2, \cdots, m-1 \\ \sqrt{\frac{1}{m}} \cos\left(\frac{\pi}{m} i \left(j + \frac{1}{2}\right)\right) & i = 0 \end{cases}. \tag{3.30}$$

DCT is applied to blocks of an image. The resulting coefficients are grouped together based on their position in the transformed matrix. Thus, the application of DCT on an image would result in the generation of different bands of coefficients. Each band of coefficient would have distinct variances, and would thereby, require different quantizers. On the other hand, within each band, all coefficients are treated equally important. Thus, within each band, the bit allocation should be equal.

3.5 Coder complexity

In this section, we consider the computational compexity of the proposed coder. The number of packets transmitted per BOV is given by L_t. The computational complexity for calculating (3.19) is given by

$$\mathbb{O}\left(L_t^2\right). \tag{3.31}$$

The values considered for frame expansion range from K to $K \times L_t$. Therefore, the number of values being considered for frame expansion is given by $[(L_t - 1)K + 1]$. Now, for each value of frame expansion being considered, the distortion is calculated for $L_t + 1$ scenarios. The computational complexity for calculating (3.22) for a source vector in the BOV is then given by

$$\begin{aligned} &[K(L_t - 1) + 1] \times \mathbb{O}(L_t) \\ &= [KL_t - K + 1] \times \mathbb{O}(L_t) \\ &= \mathbb{O}\left(KL_t^2\right). \end{aligned} \tag{3.32}$$

A linear search to find the value of expansion factor resulting in the minimum distortion would have the computational complexity given by

$$\mathbb{O}(KL_t). \tag{3.33}$$

In case of an *iid* Gaussian source, the result obtained for one source vector of the BOV is applicable to the other source vectors in the BOV. Hence, the algorithm complexity for a BOV is given by

$$\begin{aligned} &\mathbb{O}\left(L_t^2\right) + \mathbb{O}\left(KL_t^2\right) + \mathbb{O}(KL_t) \\ &= \mathbb{O}\left(KL_t^2\right). \end{aligned} \tag{3.34}$$

In case of q non identically distributed Gaussian sources, the bit allocation algorithm requries $\frac{qKr_s}{\Delta b}$ iterations to allocate the total bits available. Additionally, at each step of the iteration, the algorithm solves (3.22) for the addition of Δb bits to every source and finds

the source with the maximum reduction. The resultant algorithm complexity is given by

$$\begin{aligned}
&\mathbb{O}\left(L_t^2\right) + \frac{qKr_s}{\Delta b}\left[2q \times \left\{\mathbb{O}\left(KL_t^2\right) + \mathbb{O}\left(KL_t\right)\right\} + \mathbb{O}\left(q\right)\right] \\
&= \mathbb{O}\left(L_t^2\right) + \frac{qKr_s}{\Delta b}\left[\mathbb{O}\left(qKL_t^2\right) + \mathbb{O}\left(qKL_t\right) + \mathbb{O}\left(q\right)\right] \\
&= \mathbb{O}\left(L_t^2\right) + \mathbb{O}\left(\frac{q^2K^2L_t^2r_s}{\Delta b}\right) + \mathbb{O}\left(\frac{q^2K^2L_tr_s}{\Delta b}\right) + \mathbb{O}\left(\frac{q^2Kr_s}{\Delta b}\right) \\
&= \mathbb{O}\left(\frac{q^2K^2L_t^2r_s}{\Delta b}\right) \\
&= \mathbb{O}\left(q^2K^2L_t^2u\right)
\end{aligned} \tag{3.35}$$

where, $u = \frac{r_s}{\Delta b} \geq 1$. The encoder generates frame coefficients using (3.7) and the computational complexity is given by

$$\begin{aligned}
&\mathbb{O}\left[n\left(KL_t \times K \times 1\right)\right] \\
&= \mathbb{O}\left[nK^2L_t\right].
\end{aligned} \tag{3.36}$$

The decoder uses the pseudoinverse and the computational complexity is given by

$$\mathbb{O}\left[n\left(KL_t\right)^3\right]. \tag{3.37}$$

The analysis indicates that computational complexity (3.34) of the proposed algorithm for a *iid* Gaussian source is quadratic with respect to the number of packets being transmitted and linear with regards to the dimensionality of the source. On the other hand, the complexity (3.35) of the proposed bit allocation and code optimization algorithm is quadratic with respect to the number of the sources, the size of the source, the number of packets transmitted and linear with respect to the ratio of the bits per sample to bits allocated in every iteration.

Chapter 4

Simulation Results and Discussions

In this chapter, simulation results are presented to illustrate the performance of the proposed JSCC. The simulations presented model the transmission of SU data in cognitive radio network. The number of channels available are known to both the SU transmitter and receiver. Packet loses due to fading have been ignored in the set-up and the only cause for the loss of packet transmitted by the SU is the arrival of PU traffic on the cognitive radio channels. The performance of the proposed JSCC is compared to the performance of the following codes.

1. *Erasure Codes [16]* : The source data is quantized at a rate of $(K/N_{t,j})\, r_S$ bits producing K codewords. Erasure codes f: $\mathbb{R}^K \rightarrow \mathbb{R}^{N_{t,j}}$ converts the quantizer output to generate $N_{t,j}$ distinct outputs as shown in fig. 4.1. The decoder is able to reconstruct the source vector, when K or more symbols are received. However, erasure codes provide no benefit when more than K symbols are received. The optimization procedure used for finding the optimal redundancy $N_{t,j}$ at each transmission stage is calculated using (3.22) where the distortion measure (3.21) is modified for erasure codes and is given by

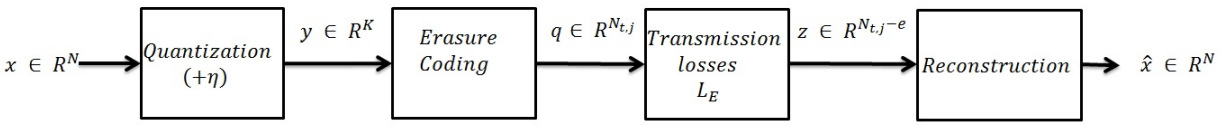

Figure 4.1: System setup using erasure codes.

$$D_{t,j}(e) = \frac{1}{K} E\left\{ \|\underline{X}_{TJ} - \underline{\hat{X}}_{TJ}\|^2 | T = t; E_t = e; J = j \right\}$$
$$= \begin{cases} \sigma_j^2 & e > N_{t,j} - K \\ D_q(b_{t,j}) & e \leq N_{t,j} - K. \end{cases} \tag{4.1}$$

where, $D_q(b_{t,j})$ is distortion of the quantizer for the rate of $b_{t,j}$ bits and e is the number of erasures for the BOV j at time instant t. The implementation of erasure codes to generate $N_{t,j}$ distinct symbols was not considered in the simulations. Instead the decoder reproduces quantized version of the input when K or more codewords were received. The performance thus achieved using erasures codes provides an upper bound for comparing the performance of the proposed JSCC.

2. *Repetitions*: The proposed JSCC is compared to a repetition codes. The expansion factor $N_{t,j}$ obtained using (3.22) is repeated $N_{t,j}/K$ times and then quantized at a rate of $(K/N_{t,j})\, r_S$ bits. Unlike the proposed JSCC, the advantage of using repetition code is that it allows the reconstruction of the source even when less that K codewords out of the transmitted $N_{t,j}$ codewords are received.

4.1 Performance of JSCC for Gaussian source

In this section, the simulation results for assessing the performance of the proposed JSCC for Gaussian sources are presented. The Gaussian data set used for these simulation has zero mean, unit variance and 2×10^6 samples. The variance and the mean of the source

vectors are known to both the encoder and decoder apriori. The sampling rate is taken to be 51200 samples per second.[1]

4.1.1 Channel parameters used

1. *Number of PUs in the network* : All simulations consider 8 PUs in the network.

2. *PU arrival rate* : In [47], it was seen that the arrival rates ranged between 0 to 500 packets per second. In our simulations, the same range has been considered. The arrival parameter when expressed in milliseconds converts to $\lambda = 0.0, 0.05, \cdots, 0.5$.

3. *Sensing time* : Fast sensing algorithms usually take less than 1 millisecond [56]. Therefore, the sensing time is taken to be 1 millisecond, *i.e.*, $T_S = 1$.

4. *Dimensionality of the source vector* : The frame operator matrix is $N_{t,j} \times K$ in size. Using a higher dimensional source vector would increases the computational complexity ($\mathbb{O}^{n^3}$) of matrix inversions required for decoding. The source vector is therefore taken to be 2-dimensional, *i.e.*, $\underline{X}_{t,j} \in \mathbb{R}^2$

5. *Transmission rate* : The transmission rate is fixed at 8 bits/sample. $r_S = 8$

6. *Packet size* : Under the varying conditions of a cognitive radio environment, short packet sizes would perform better and would decrease the possibility of PU interference but would however require extensive overhead due to headers and trailers in each packet. On the other hand, larger packet sizes would improve the throughput but would increase the packet loss probability due to PU collisions. In our simulations, a packet size of 40 bytes is considered, as used in Skype [57]. The header is taken to be 8 bytes leaving 32 bytes for the payload.

7. *BOV Size* : Each packet at the most can carry K frame coefficients of a source vector.

[1] A standard audio sampling rate widely used in profession digital video equipments is 48000 Hz, *i.e.*, 48000 samples are transmitted every second [55].

The BOV size is therefore given by

$$n = \frac{l-h}{K} = \frac{320-64}{2} = 128 \text{ source vectors.} \tag{4.2}$$

8. *Channel capacity* : Each PU channel capacity is assumed to be 128 kbps.

9. *Data transmission phase* : At a sampling rate of 51200 sample per seconds, the generation of 128 2-dimensional source vectors, or 256 samples would require 5 milliseconds. With a constant sensing time of 1 milliseconds and using (3.8), where $T_S + T_T = T_{Gen}$, the transmission time available for the Gaussian samples is given by $T_T = 4$ milliseconds.

4.1.2 Code performance for *iid* Gaussian source

Fig. 4.2*a* illustrates the performance of the proposed JSCC against the the repetitive code using uniform quantizer. It is seen that the JSCC outperforms the repetitive code and

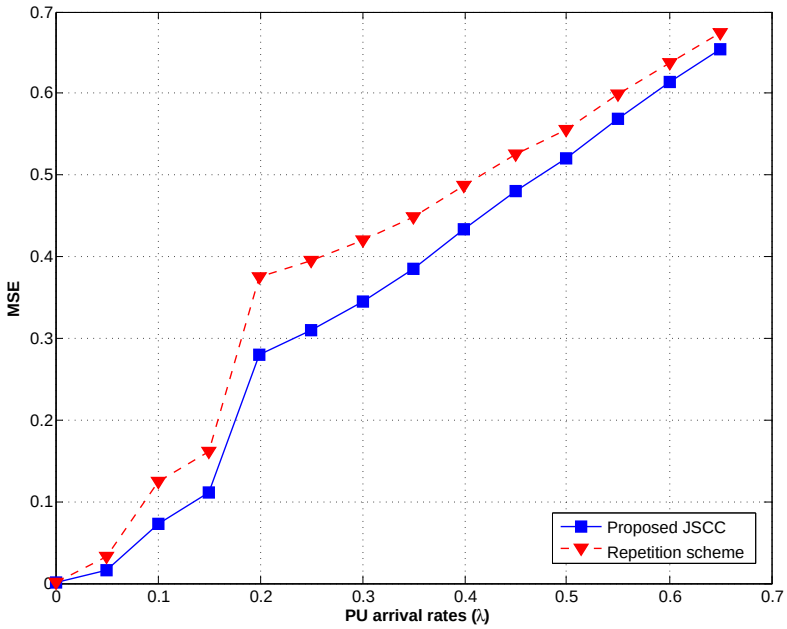

(a) Uniform quantizer.

Figure 4.2: Distortion of the proposed JSCC and repetition code for a unit-variance, zero-mean *iid* Gaussian source vector (*contd.*)

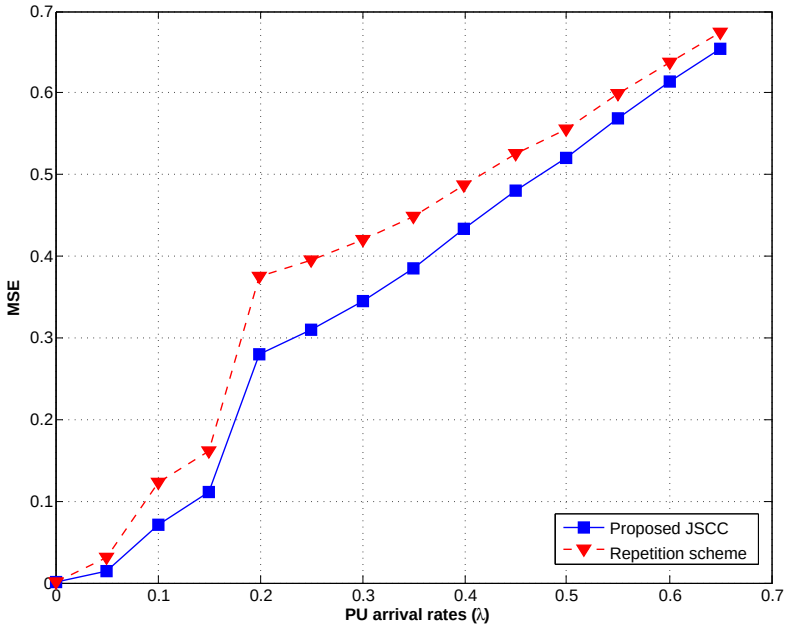

(b) Non-uniform quantizer.

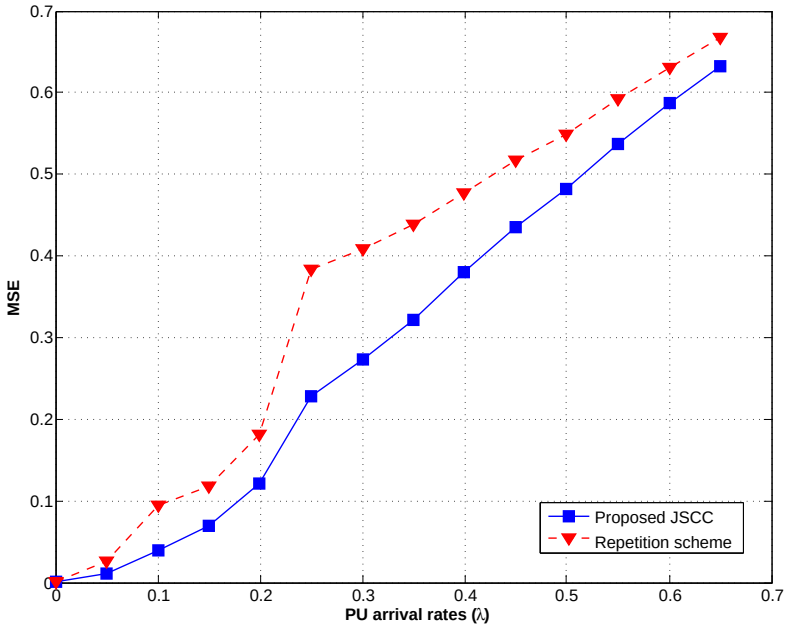

(c) Entropy constrained quantizer.

Figure 4.2: Distortion of the proposed JSCC and repetition codes for a unit-variance, zero-mean *iid* Gaussian source vector.

achieves lower distortion. Unlike repetitive codes, the JSCC estimates the source by its mean if less than K codewords are received for a source vector. However, the lower distortion achieved by the proposed JSCC is attributed to the fact that receiving more than K codewords provides extra information about the source vector when using the proposed JSCC, yeilding a lower overall distortion. The results also show a sudden rise in MSE for the proposed JSCC at $\lambda = 0.2$. The reason for such an abrupt rise is due to the change in the bits allocated per codeword by the JSCC. At $\lambda = 0.15$, the proposed JSCC allocates 2 bits per codeword (See Fig. $4.5a$), whereas at $\lambda = 0.2$, the codewords are assigned 1 bit resulting in the sharp rise of the MSE. As shown in figs. $4.2b$ and $4.2c$, the JSCC outperforms the repetition code when non-uniform and entropy constrained quantizers are used.

The application of frame expansions in the proposed JSCC assumes (2.19) and (2.20) hold for the quantized noise components. When (2.19) and (2.20) hold, the distortion induced if the lost coefficients are orthogonal to each other is given by (2.27) while that if

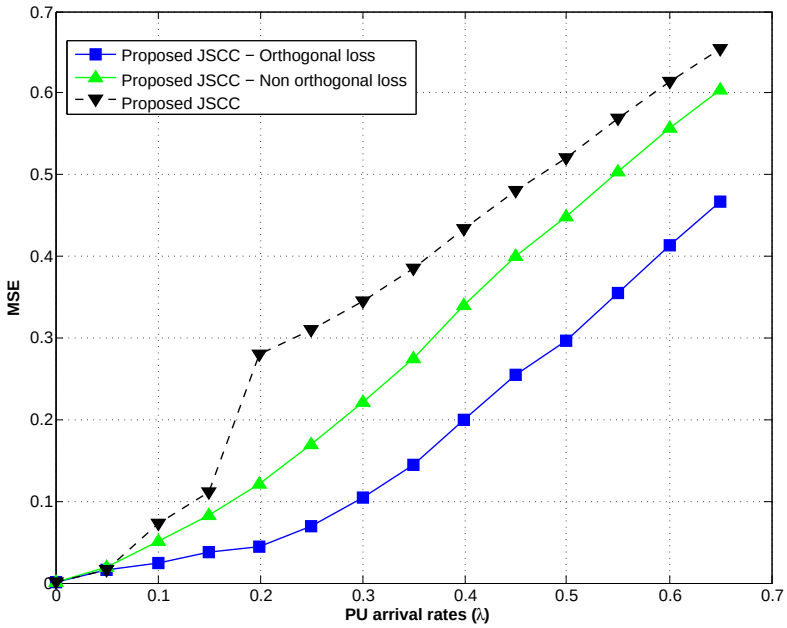

(a) Uniform quantizer.

Figure 4.3: Distortion of the proposed JSCC with (i) uncorrelated quantization noise error & orthogonal codewords lost (ii) uncorrelated quantization noise error & non orthogonal codewords lost and (iii) correlated quantization noise for a unit-variance, zero-mean *iid* Gaussian source vector (*contd.*)

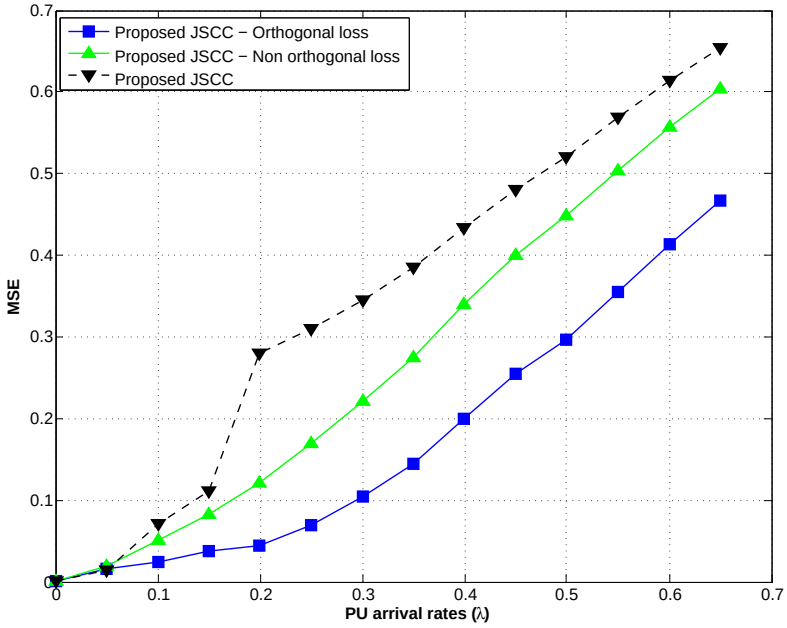

(b) Non-uniform quantizer.

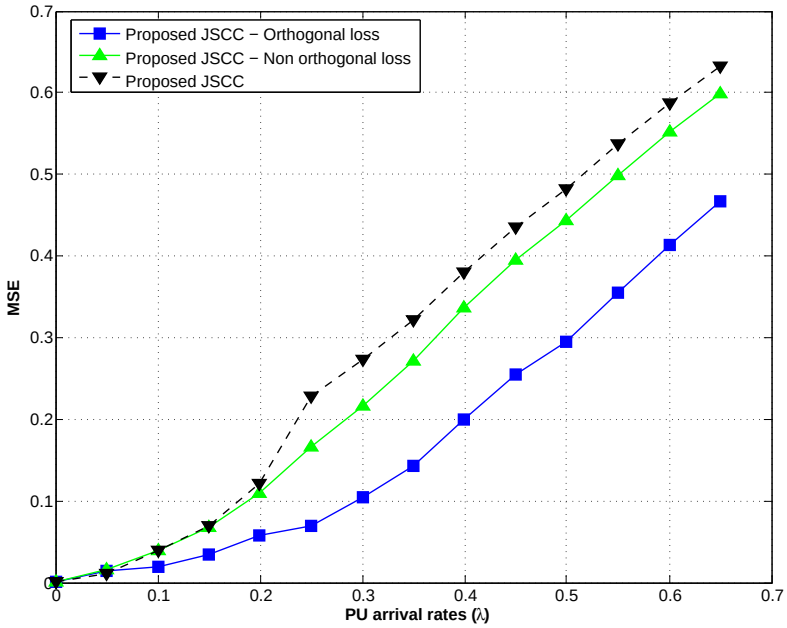

(c) Entropy constrained quantizer.

Figure 4.3: Distortion of the proposed JSCC with (i) uncorrelated quantization noise error & orthogonal codewords lost (ii) uncorrelated quantization noise error & non orthogonal codewords lost and (iii) correlated quantization noise for a unit-variance, zero-mean *iid* Gaussian source vector

the lost coefficients are non-orthogonal to each other is given by (2.26). Fig. 4.3a illustrates the performance of the proposed JSCC with uniform quantizers under three different conditions.

- (2.19) and (2.20) hold and the losses are strictly orthogonal.
- (2.19) and (2.20) hold and the losses are not necessarily orthogonal.
- (2.19) and (2.20) do not hold and the losses are not necessarily orthogonal.

The results give a clear indication that if the quantization noise components were strictly independent of the input and are uncorrelated, the MSE can be reduced. Moreover, it reaffirms the fact that orthogonal losses would achieve a better performance for the proposed JSCC. Similar results were obtained for non-uniform quantizers and entropy constrained quantizer as shown in figs. 4.3b and 4.3c.

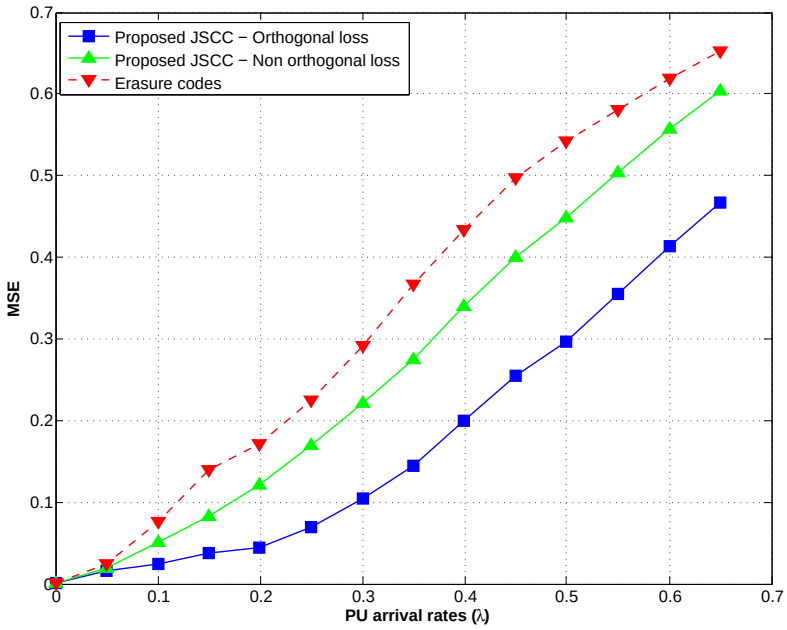

(a) Uniform quantizer.

Figure 4.4: Distortion of the proposed JSCC with (i) uncorrelated quantization noise error & orthogonal codewords lost (ii) uncorrelated quantization noise error & non orthogonal codewords lost and (iii)erasure codes for a unit variance-zero mean *iid* Gaussian source vector (*contd.*)

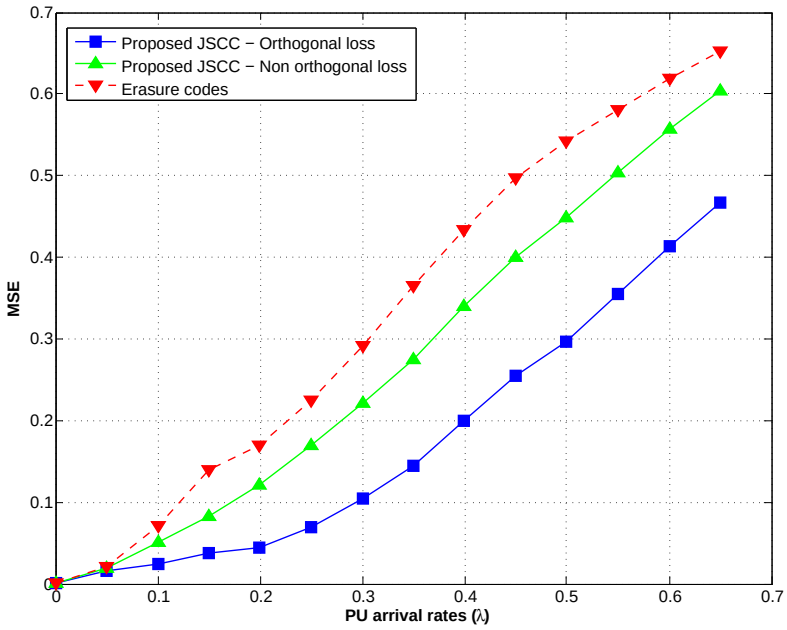

(b) Non-uniform quantizer.

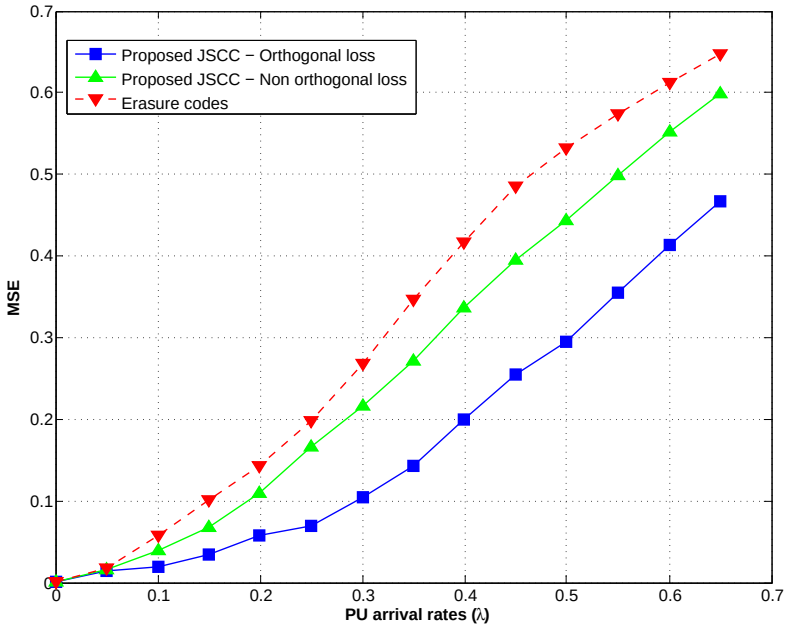

(c) Entropy constrained quantizer.

Figure 4.4: Distortion of the proposed JSCC with (i) uncorrelated quantization noise error & orthogonal codewords lost (ii) uncorrelated quantization noise error & non orthogonal codewords lost and (iii) erasure for a unit variance-zero mean *iid* Gaussian source vector

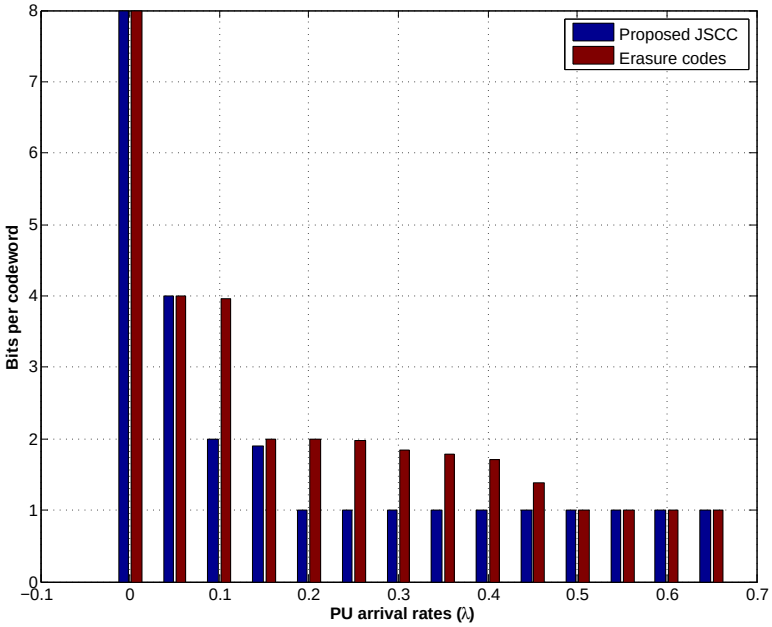

(a) Uniform quantizer.

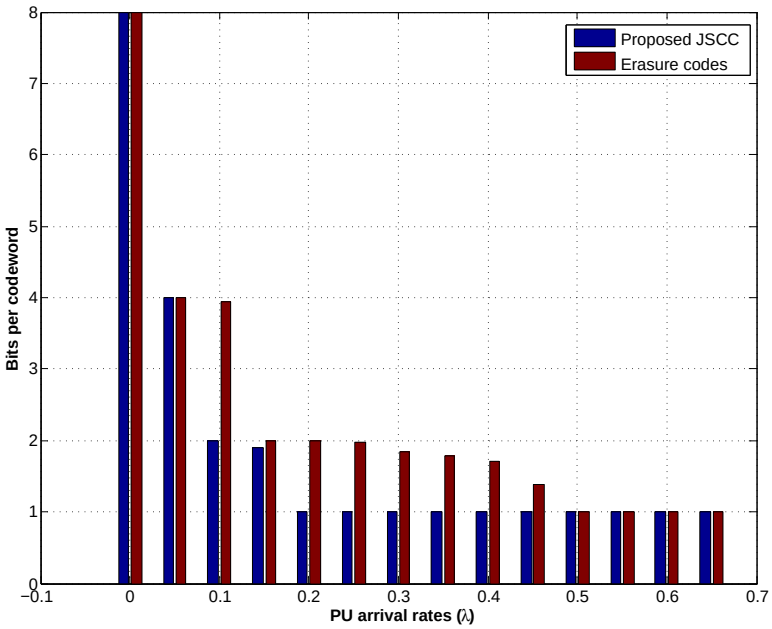

(b) Non-uniform quantizer.

Figure 4.5: Bit allocation per codeword using proposed JSCC and erasure codes (*contd.*)

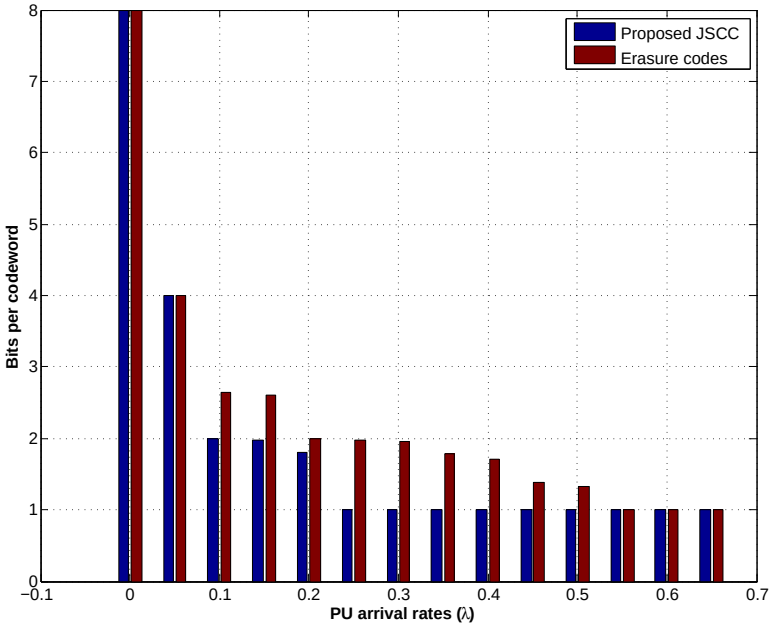

(c) Entropy constrained quantizer.

Figure 4.5: Bit allocation per codeword using proposed JSCC and erasure codes

As shown in fig. $4.4a$, $4.4b$, and $4.4c$, the proposed JSCC outperforms erasure codes under the conditions.

- (2.19) and (2.20) hold and the losses are strictly orthogonal.
- (2.19) and (2.20) hold and the losses are not necessarily orthogonal.

However, as it can be clearly seen from fig. $4.3a$ and $4.4a$, when (2.19) and (2.20) do not hold the proposed JSCC does not necessarily outperform erasure codes at lower rates as the quantization noise is correlated and results in higher MSE.

4.1.3 Code and proposed bit allocation algorithm performance for non identically distributed Gaussian sources

The bit allocation algorithms discussed in sec. $3.3.2$ are tested for 4 different Gaussian sources with zero mean and different standard deviations $\sigma_1, \cdots, \sigma_4$. 100 different combinations of $\sigma_1, \cdots, \sigma_4$ are considered for the simulation. Since the optimal bit allocation

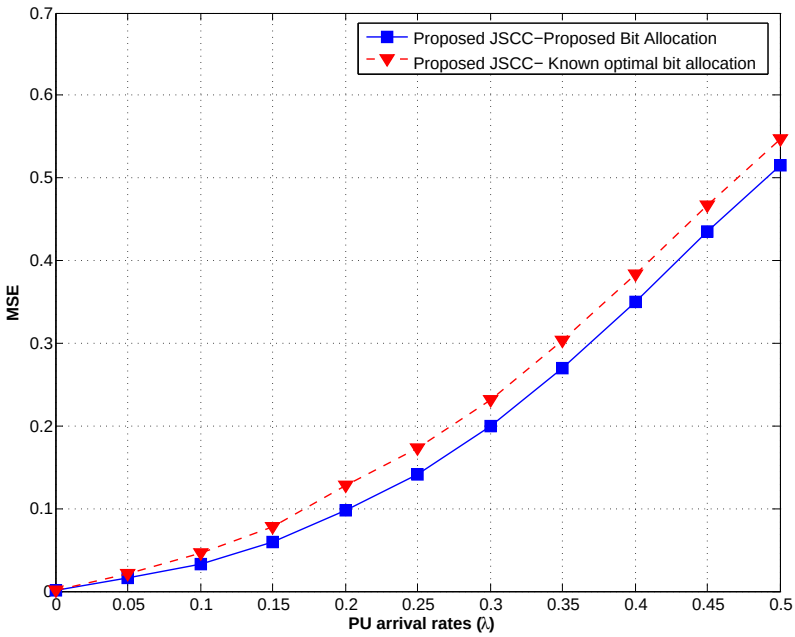

(a) Conditional MSE

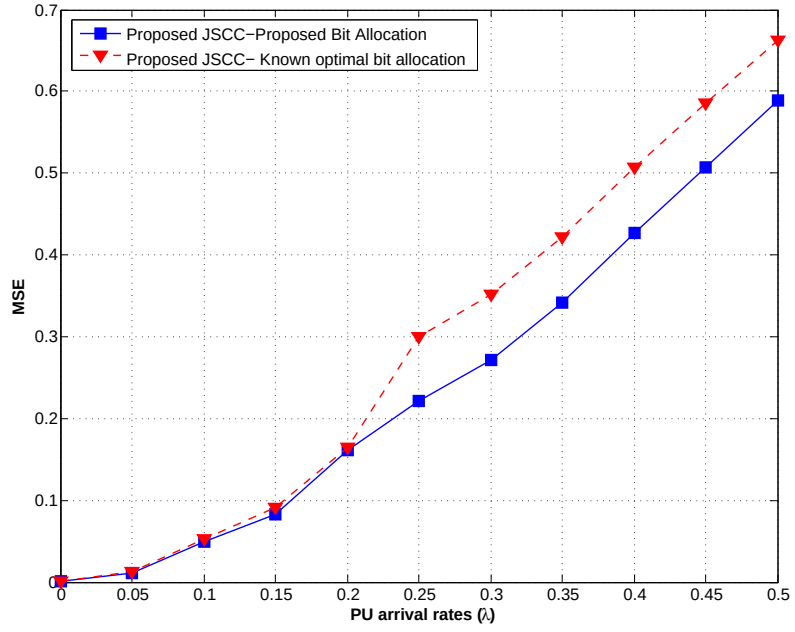

(b) Actual MSE

Figure 4.6: Distortion of the proposed JSCC using proposed bit allocation and optimal bit allocation strategy

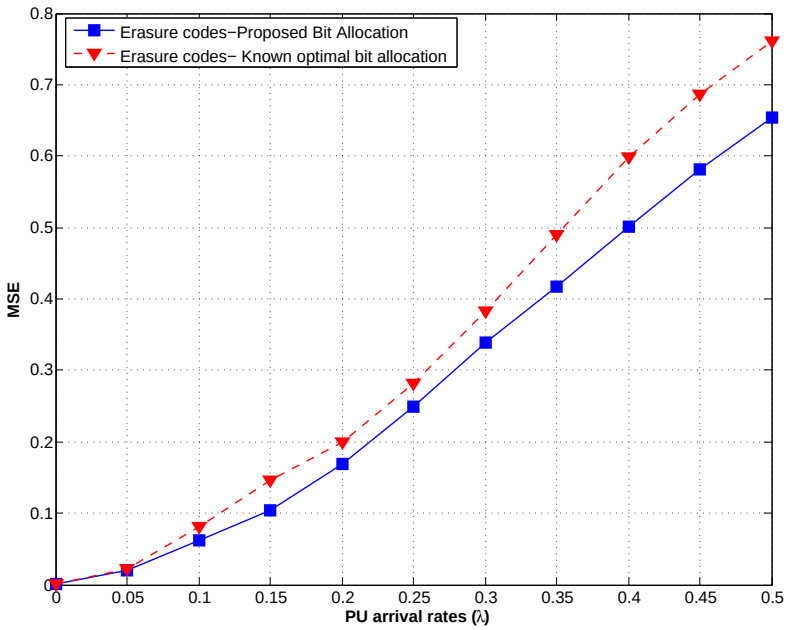

(a) Conditional MSE

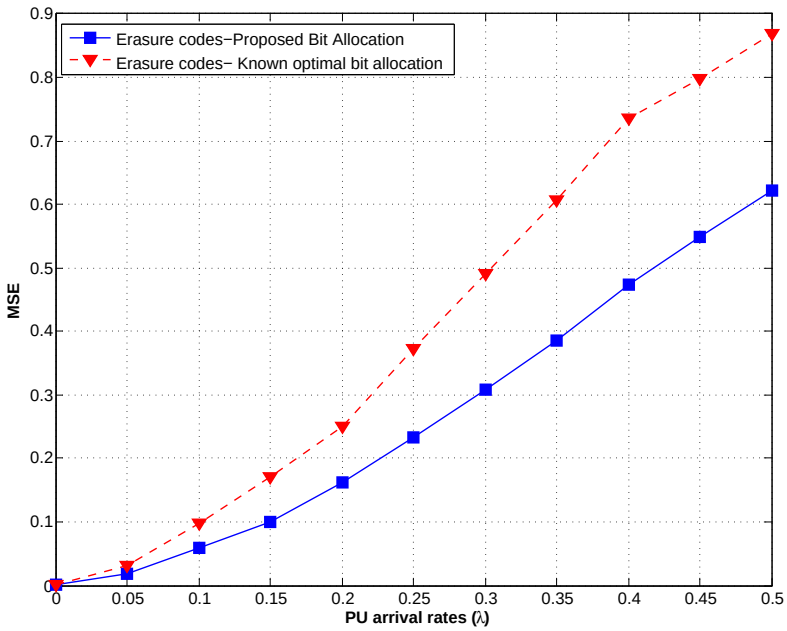

(b) Actual MSE

Figure 4.7: Distortion of erasure codes using proposed bit allocation and optimal bit allocation strategy

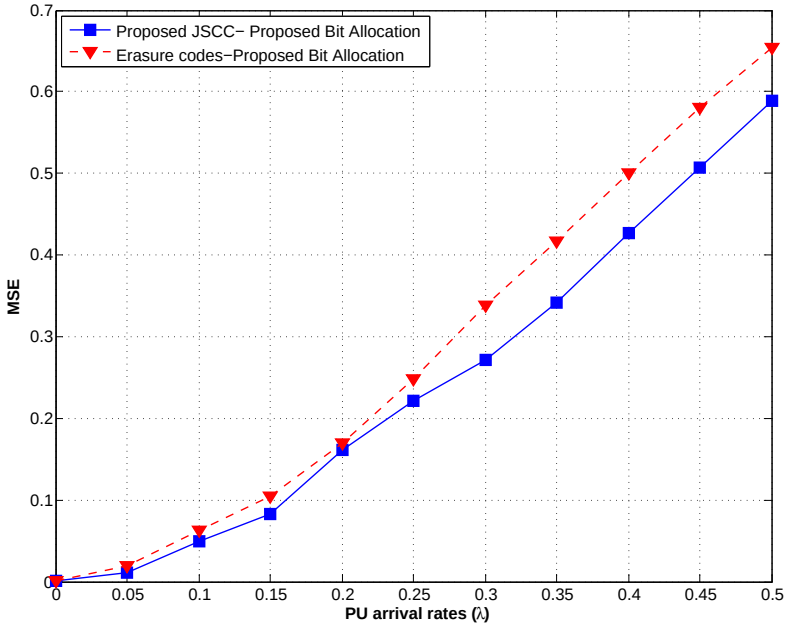

(a) Comparison of MSE achieved for proposed JSCC and erasure codes.

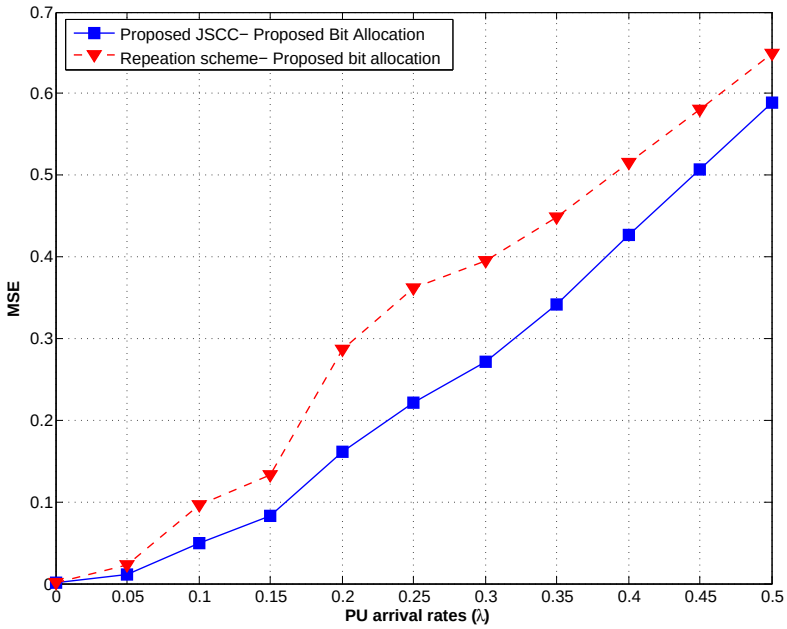

(b) Comparison of MSE achieved for proposed JSCC and repetition code.

Figure 4.8: Distortion of the proposed bit allocation for proposed JSCC, erasure codes and repetition codes

would result in non-integer bit allocations, fixed rate quantizers cannot be used and we compare the two algorithm for entropy constrained quantizers. Fig. $4.6a$ shows the performance of the proposed bit allocation algorithm to that of optimal bit allocation. The optimal bit allocation algorithm focusses on minimizing the overall distortion due to the quantizer but does not minimize the (3.22). On the other hand, the proposed algorithm finds a simple solution that minimizes (3.22) and can be incorporated into the proposed JSCC.

The overall distortion achieved by the JSCC using the proposed bit allocation algorithm was found to be lower than the distortion achieved using the optimal bit allocation solution when implemented for the transmission of non identically distributed Gaussian source vectors as shown in fig. $4.6b$. Similar results were obtained when the proposed bit allocation was applied to erasure codes as shown in fig. 4.7. Comparing the performances of the proposed JSCC and the erasure codes, it is found that the JSCC outperforms erasure codes and the repetition code using the proposed bit allocation algorithms as presented in fig. 4.8

4.2 Performance of JSCC for image

Figure 4.9: Grayscale Lena image.

In this section, we present simulation results obtained by applying the JSCC to image transmission. In addition to MSE, we also present the peak signal to noise ratio (PSNR) for the images received at the decoder. As the bit rates (in bits per pixel) in image coding is typically fractional, we only consider entropy coded quantization. The transmission of grayscale 512×512 Lena and 256×256 Mandrill image as shown in figs. 4.9 and 4.10 are considered. We consider two different scenarios for the transmission of images.

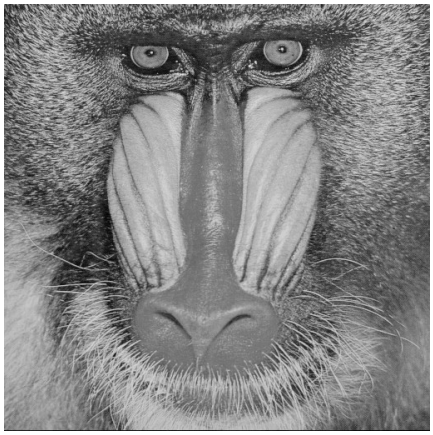

Figure 4.10: Grayscale Mandrill image.

4.2.1 Case I : One BOV per transmission period

In the section, we present simulation results obtained by applying the JSCC to image transmission and transmitting only one BOV per transmission period. The channel parameters discussed in $4.1.1$ have been considered for these simulations as well.

Performance with direct encoding of pixels

The image is transmitted by applying JSCC to image pixels directly. The MSE and PSNR obtained for Lena and Mandrill images as shown in figs. 4.11, 4.15, 4.12 and 4.16 respectively, clearly indicate that the JSCC outperforms both the repetitive and erasure codes. The bits allocated per codeword for JSCC and erasure codes for Lena and Mandrill images have been shown in figs. 4.14 and 4.17. Figs. 4.13 and 4.18 illustrates the reconstruction

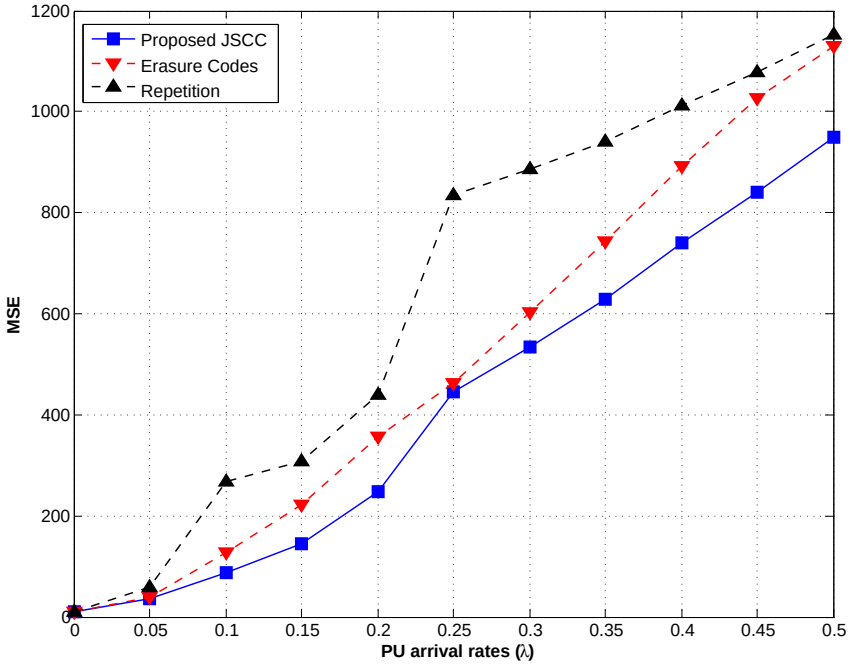

Figure 4.11: Comparison of MSE using proposed JSCC, repetition and erasure codes for the transmission of Lena image without transform coding.

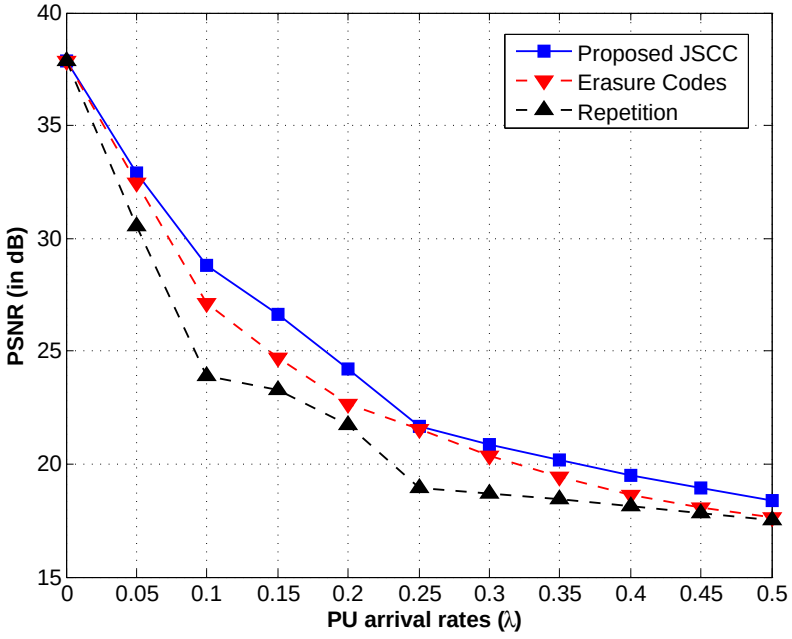

Figure 4.12: Comparison of PSNR using proposed JSCC, repetition and erasure codes for the transmission of Lena image without transform coding.

(a) Proposed JSCC

(b) Erasure Codes

(c) Repetition

Figure 4.13: Reconstructed image of Lena at $\lambda = 0.10$ for proposed JSCC, erasure and repetition code

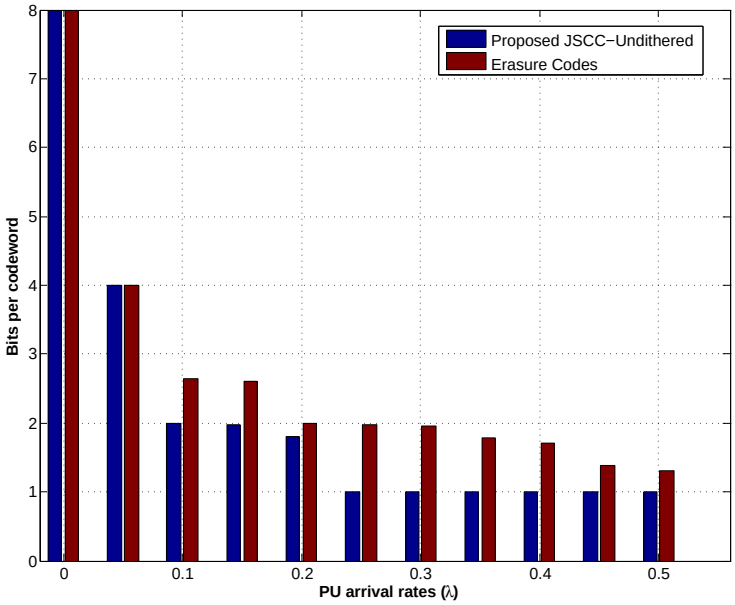

Figure 4.14: Bit allocated per codeword using proposed JSCC and erasure codes for the transmission of Lena image without transform coding.

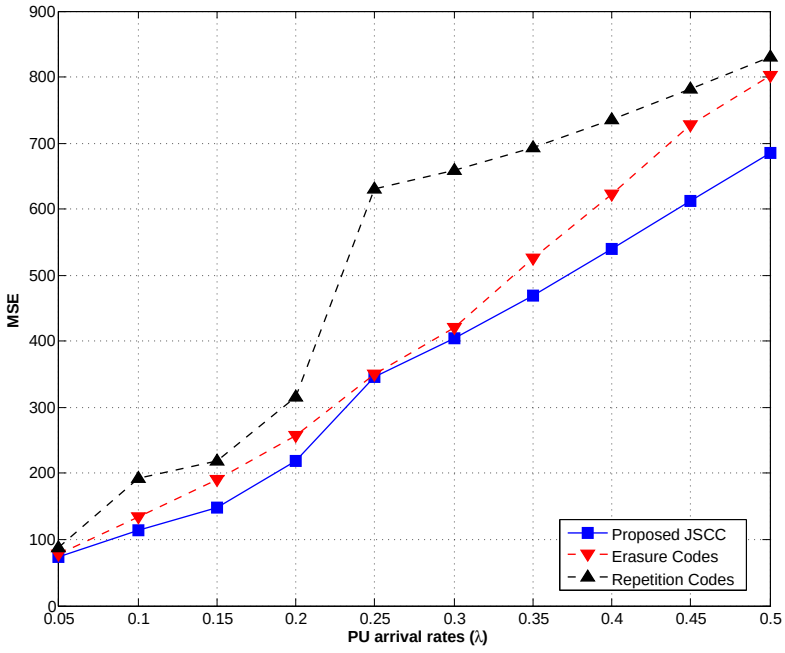

Figure 4.15: Comparison of MSE using proposed JSCC, repetition and erasure codes for the transmission of Mandrill image without transform coding.

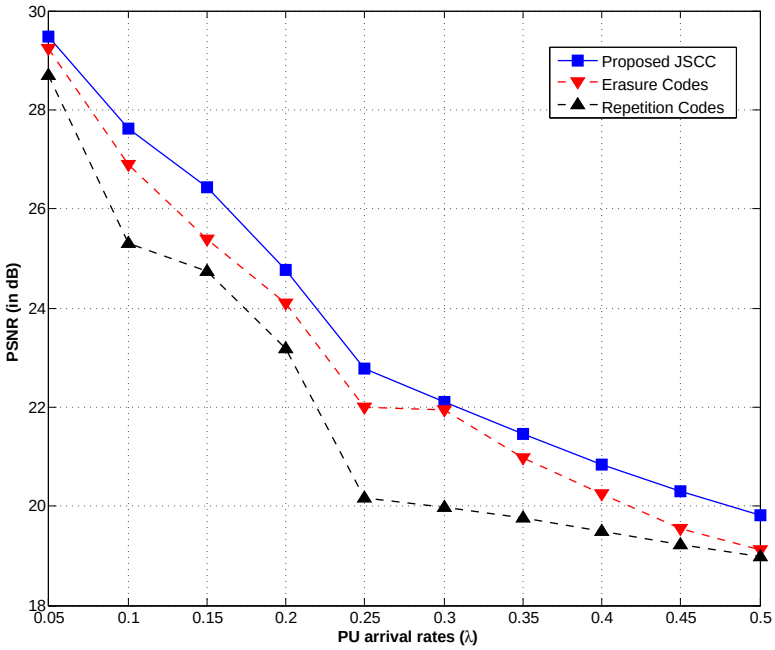

Figure 4.16: Comparison of PSNR using proposed JSCC, repetition and erasure codes for the transmission of Mandrill image without transform coding.

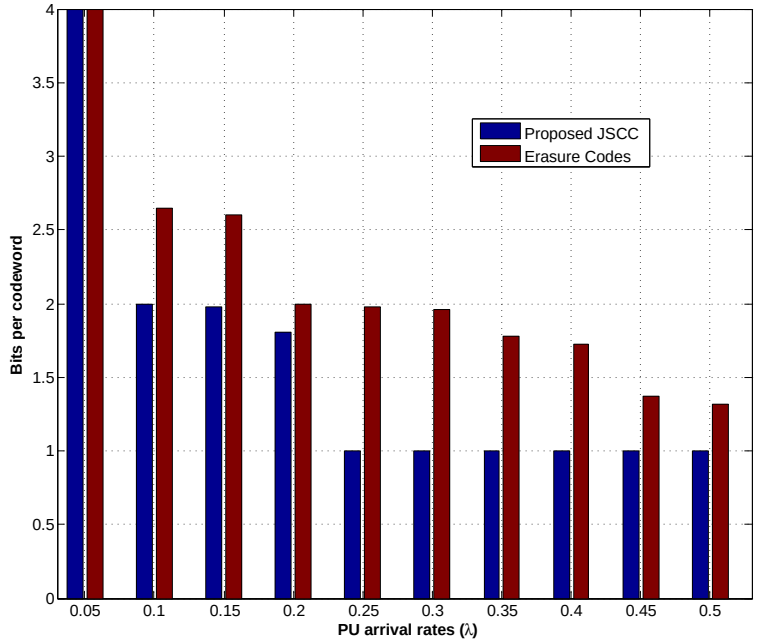

Figure 4.17: Bit allocated per codeword using proposed JSCC and erasure codes for the transmission of Mandrill image without transform coding.

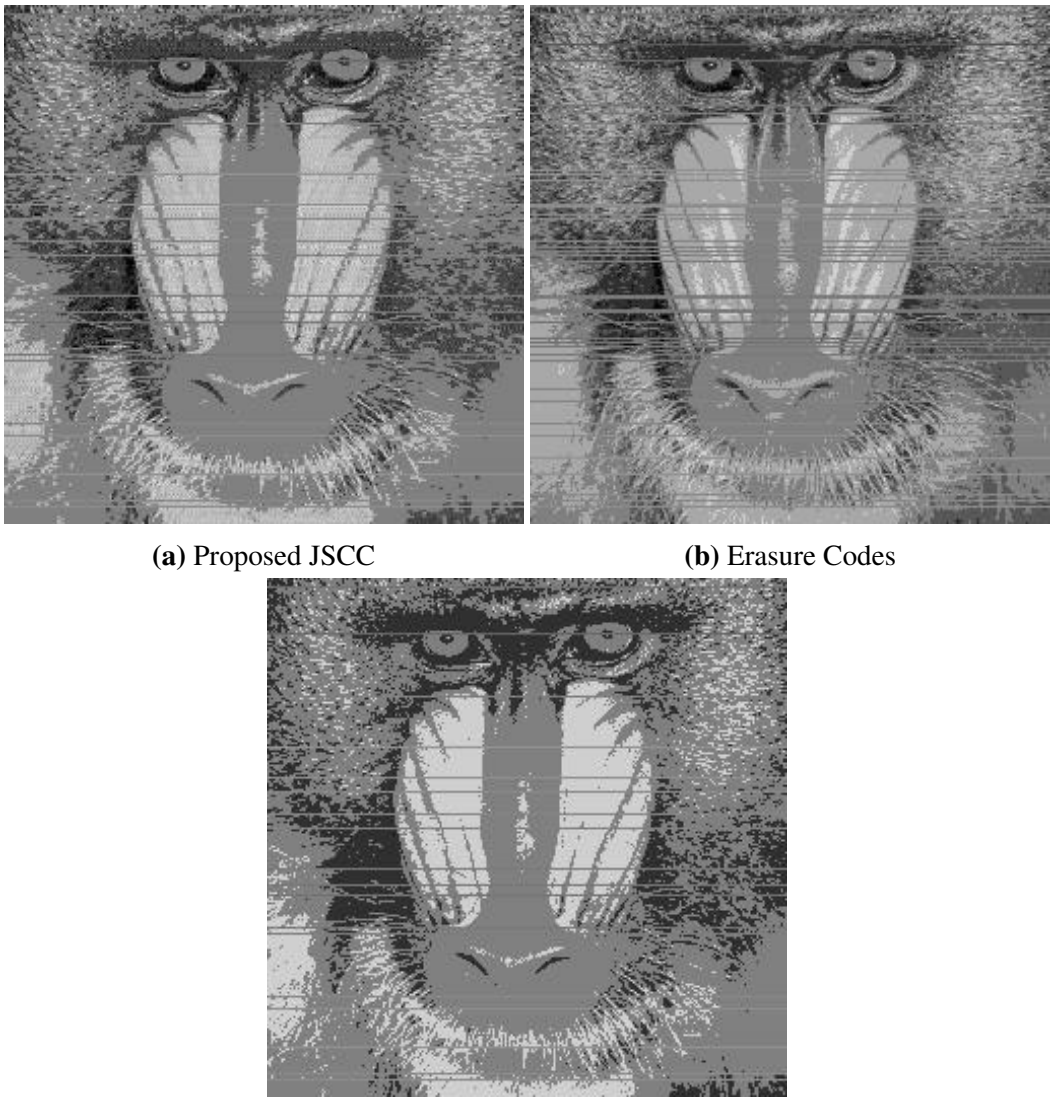

(a) Proposed JSCC **(b)** Erasure Codes

(c) Repetition

Figure 4.18: Reconstructed image of Mandrill at $\lambda = 0.20$ for proposed JSCC, erasure and repetition code

of Lena image at PU arrival rate of 0.10 and the reconstruction of Mandrill image at PU arrival rate of 0.20 respectively. As seen in the results, the reconstructed image using the JSCC is perceptually better than the image reconstructed using erasure code or repetition code.

Performance for transmission of transform coded image

The MSE and PSNR of the JSCC and erasure codes for Lena image is presented in figs. 4.19 and 4.20 respectively. While the MSE and PSNR are very close in both cases for the

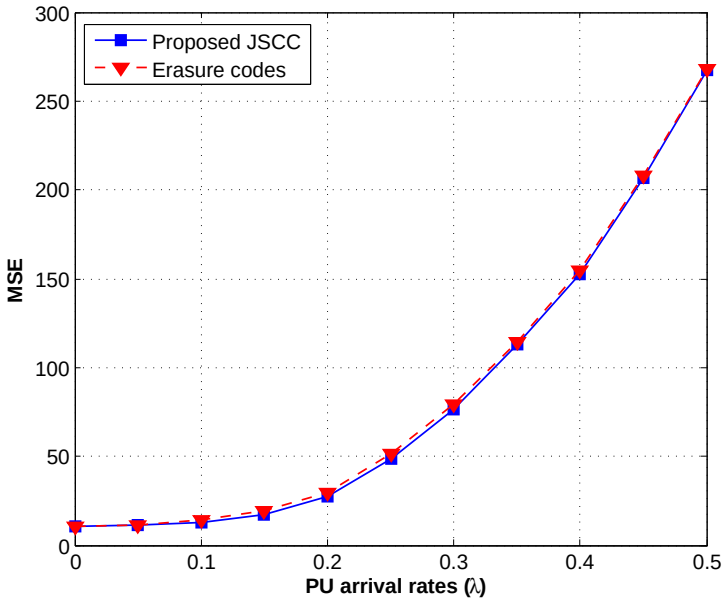

Figure 4.19: Comparison of MSE using proposed JSCC and erasure codes for the transmission of Lena image with transform coding.

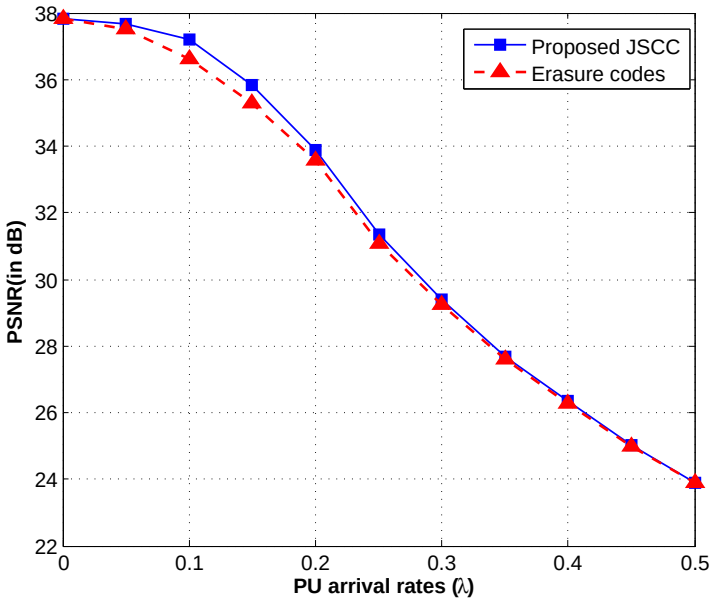

Figure 4.20: Comparison of PSNR using proposed JSCC and erasure codes for the transmission of Lena image with transform coding.

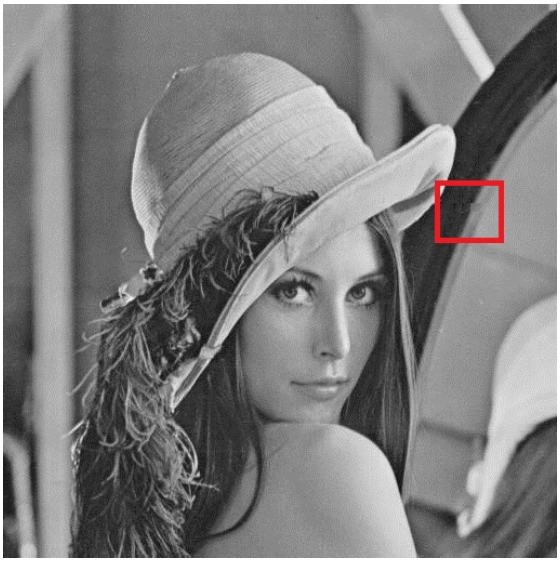

(a) Proposed JSCC

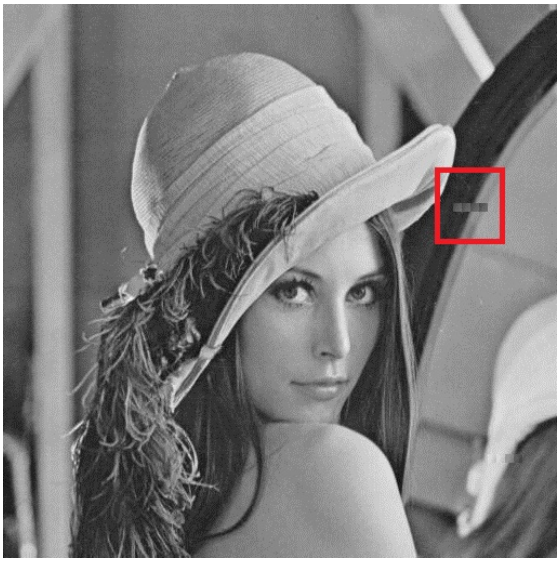

(b) Erasure Codes

Figure 4.21: Reconstructed image of Lena at $\lambda = 0.15$ for proposed JSCC and erasure codes.

Lena image, the results obtained indicate that the JSCC performs better at higher rates. Fig. 4.21 gives a better sense of the performance of the JSCC for Lena image. The background shown in red box has less distortion for the proposed JSCC than erasure codes.

When the codes were applied for Mandrill image, the results were similar. The MSE and PSNR, shown in figs. 4.22 and 4.23 respectively, again were better for the JSCC compared to the erasure codes. The reconstructed image shown in fig. 4.24 (see red box) also shows that the JSCC produces less distortion

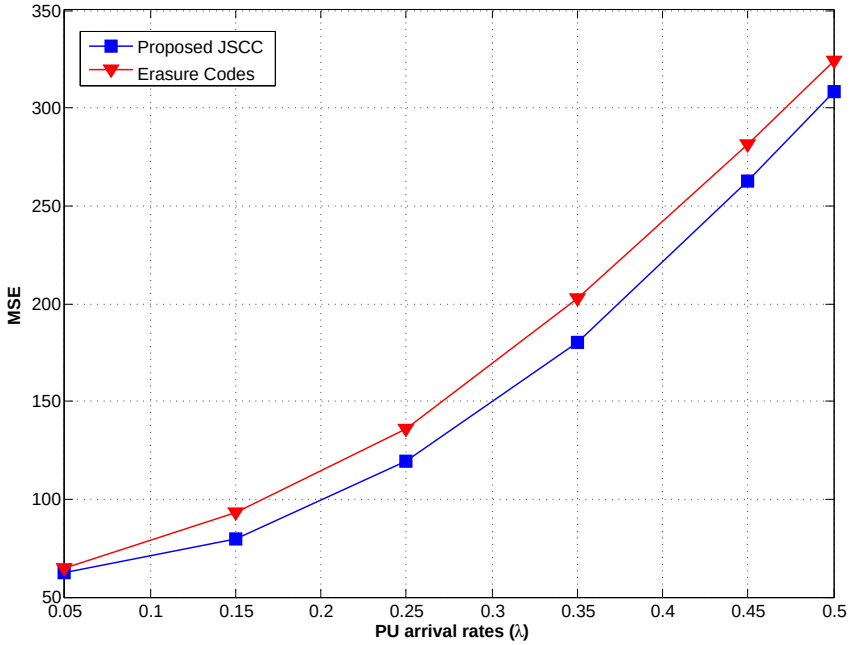

Figure 4.22: Comparison of MSE using proposed JSCC and erasure codes for the transmission of Mandrill image with transform coding.

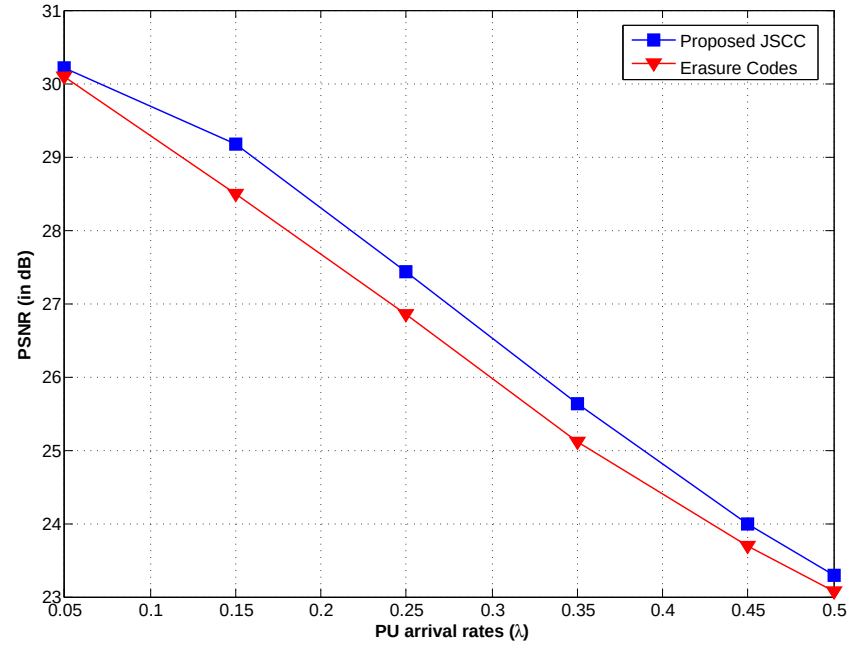

Figure 4.23: Comparison of PSNR using proposed JSCC and erasure codes for the transmission of Mandrill image with transform coding.

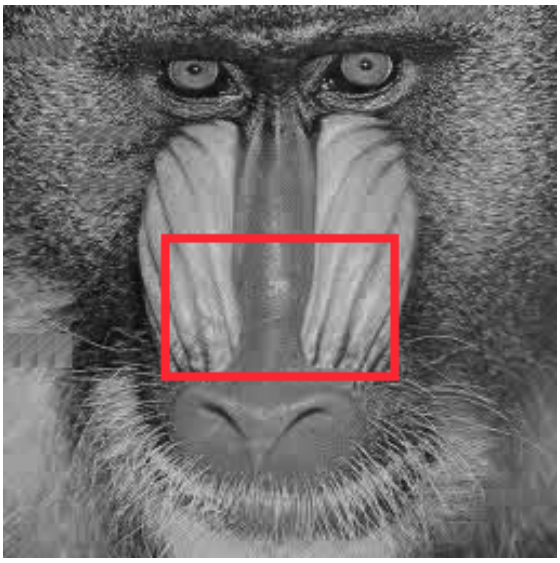

(a) Proposed JSCC

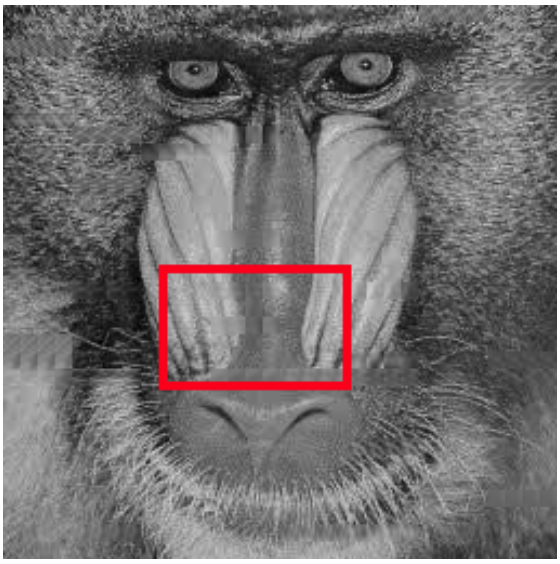

(b) Erasure Codes

Figure 4.24: Reconstructed image of Mandrill at $\lambda = 0.25$ for proposed JSCC and erasure codes.

4.2.2 Case II : Multiple BOV per transmission period

Motion pictures usually have a rate of 24 frames per second (fps). The maximum allowable delay for the transmission of a frame at a rate of 24 fps would therefore approximately be 40 ms. Unlike sec. 4.2.1, the maximum transmission delay allowed is fixed to be 40 ms. Video transmissions have coded progressive frames (also known as group of pictures) that are transmitted. However, in our simulations, we do not consider coded successive frames

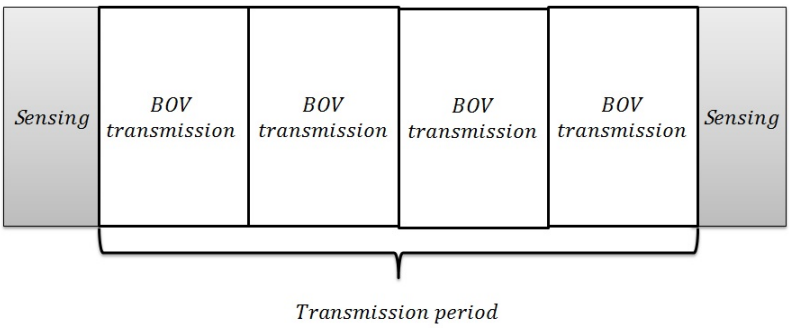

Figure 4.25: Multiple BOV during each transmission period setup.

but instead consider the transmission of still images. The packet size is taken to be 1316 bytes while the header is 292 bytes [2]. The channel capacity is taken to 10 Mbps and the PU arrival rate are considered in the range of $\lambda = 0.05, \cdots, 0.5$. The sensing time is again taken to be 1 ms. The BOV size is given by $n = \frac{l-h}{K} = \frac{10528-2336}{2} = 4096$. Without a data generation rate, the transmission period is fixed to be 4 milliseconds. Therefore, during each transmission period, 4 BOVs would be transmitted during the transmission phase using the sensing result obtained at the beginning of the transmission period as shown in fig. 4.25. With sensing limited to the beginning of the transmission period, the code optimization result obtained for the first BOV are applied to the remaining BOV in the transmission period. In the results presented hereafter, we consider the transmission of Lena and Mandrill image with the conditions imposed as above.

Direct transmission of image pixels

The MSE and PSNR achieved for direct transmission of the pixels of Lena image using the proposed JSCC and erasure codes is shown in figs. 4.26 and 4.27 respectively. Reconstructed Lena images at $\lambda = 0.15$ (shown in fig. 4.28) clearly shows that the JSCC is better able to cope with losses. Unlike erasure codes, the JSCC reproduces an image with less distortions and a higher perceptual quality.

The simulation was repeated for the transmission of the Mandrill image pixels. The

[2] In [58], it was found that packet sizes for Motion JPEG are usually consistent at 1316 bytes.

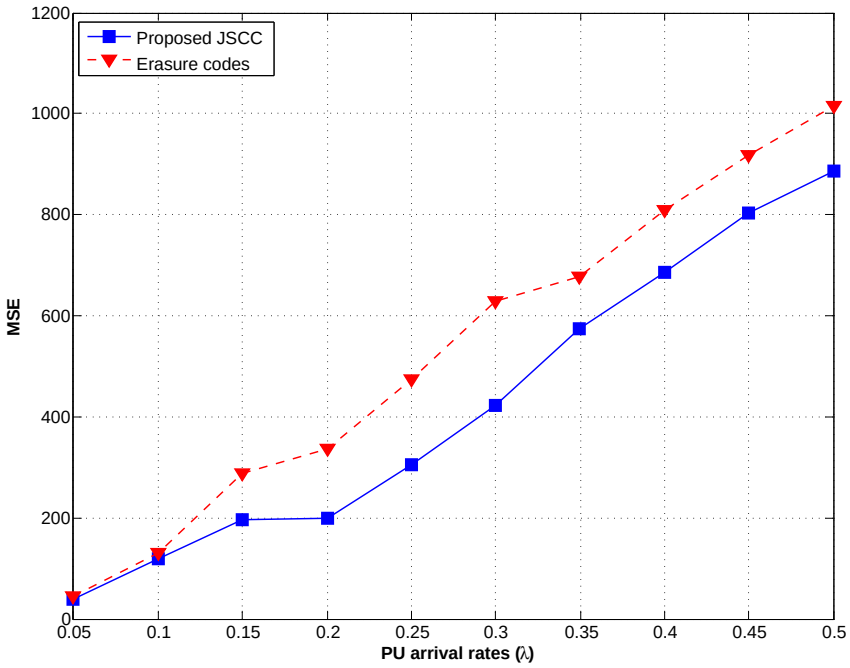

Figure 4.26: Comparison of MSE using JSCC and erasure codes for the transmission of Lena image without transform coding.

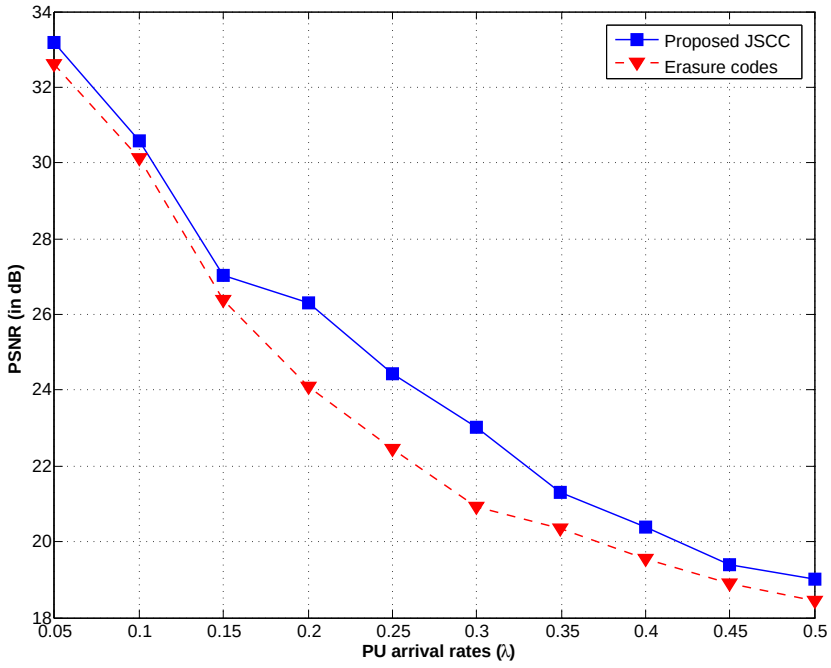

Figure 4.27: Comparison of PSNR using JSCC and erasure codes for the transmission of Lena image without transform coding.

(a) JSCC

(b) Erasure Codes

Figure 4.28: Reconstructed image of Lena at $\lambda = 0.20$ for proposed JSCC and erasure codes.

MSE and PSNR obtained (See figs. 4.29, 4.30) for the Mandrill image also show that the proposed JSCC performs better than the erasure codes. The reconstructed images shown in fig. 4.31 reconfirms that JSCC is better able to adapt to the varying conditions of the cognitive radio network and suffer less losses.

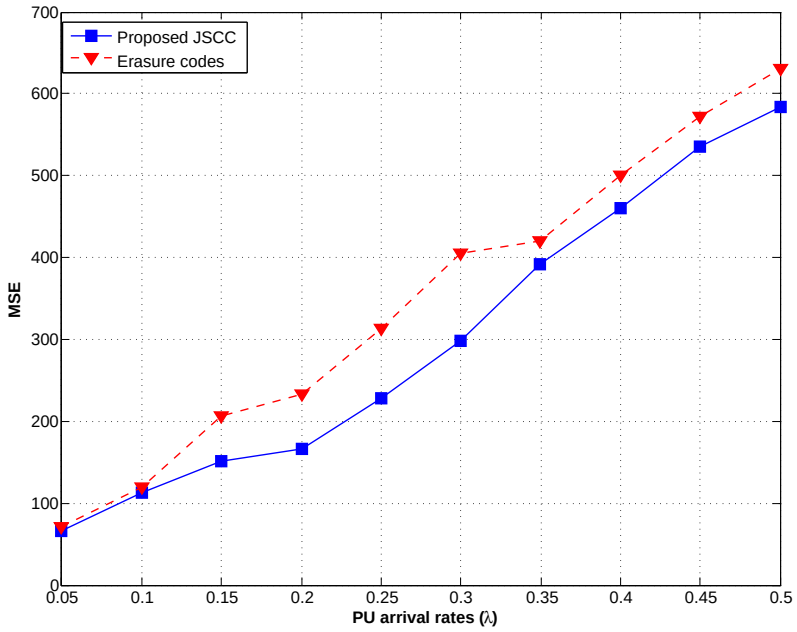

Figure 4.29: Comparison of MSE using JSCC and erasure codes for the transmission of Mandrill image without transform coding.

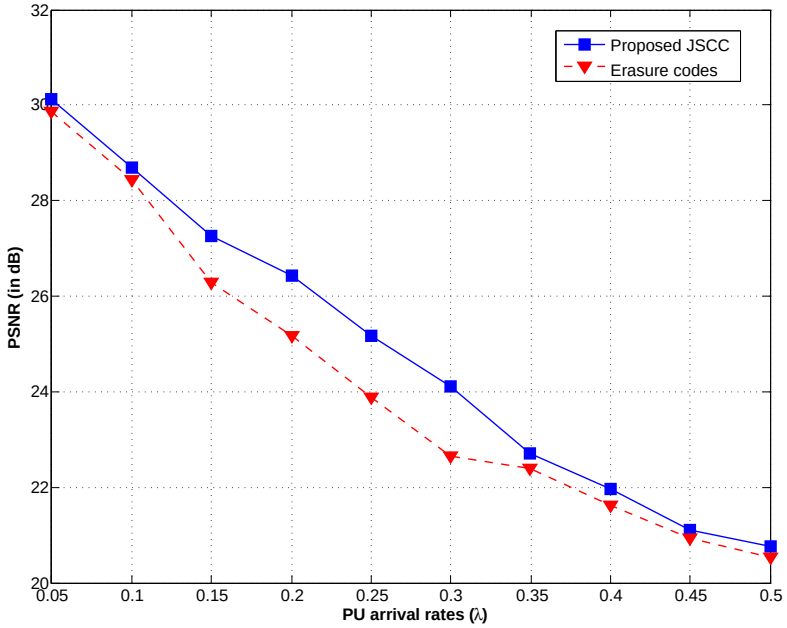

Figure 4.30: Comparison of PSNR using JSCC and erasure codes for the transmission of Mandrill image without transform coding.

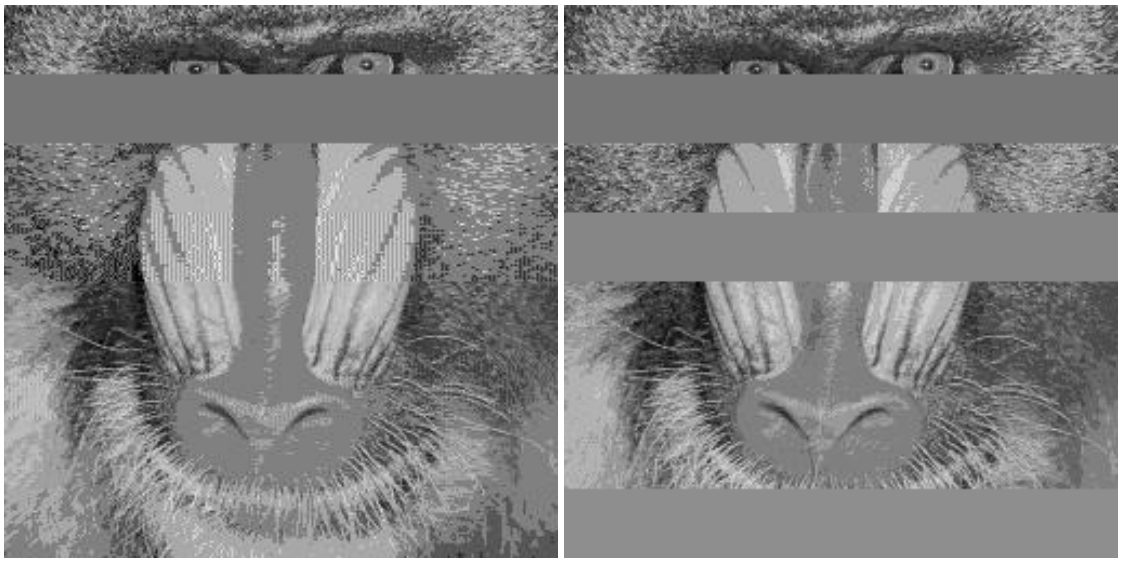

(a) JSCC **(b)** Erasure Codes

Figure 4.31: Reconstructed image of Mandrill at $\lambda = 0.20$ for proposed JSCC and erasure codes.

Transmission of DCT coefficients

The MSE and PSNR achieved using the JSCC and erasure code for transform coded Lena image using the proposed bit allocation algorithm are shown in figs. 4.32 and 4.33. Reconstructed Lena images at $\lambda = 0.20$ and $\lambda = 0.35$ are shown in figs. 4.34 and 4.35 respectively. While the graphs do indicate the superior performance of the JSCC, the difference between the performance of the JSCC and erasure codes can also be seen in the reconstructed image. When losses occur, JSCC is able to reproduce a distorted version of the image unlike erasure codes which fail.

The application of the proposed JSCC and erasure codes using the proposed bit allocation algorithm for transform coded Mandrill image also indicate the JSCC performs better than erasure code. Figs. 4.36 and 4.37 respectively shows that the JSCC achieves a lower distortion and better PSNR than erasure codes. Reconstructed Mandrill images for $\lambda = 0.35$ and $\lambda = 0.50$ (figs. 4.38 and 4.39 respectively) shows the superior perceptual quality attained using the proposed JSCC.

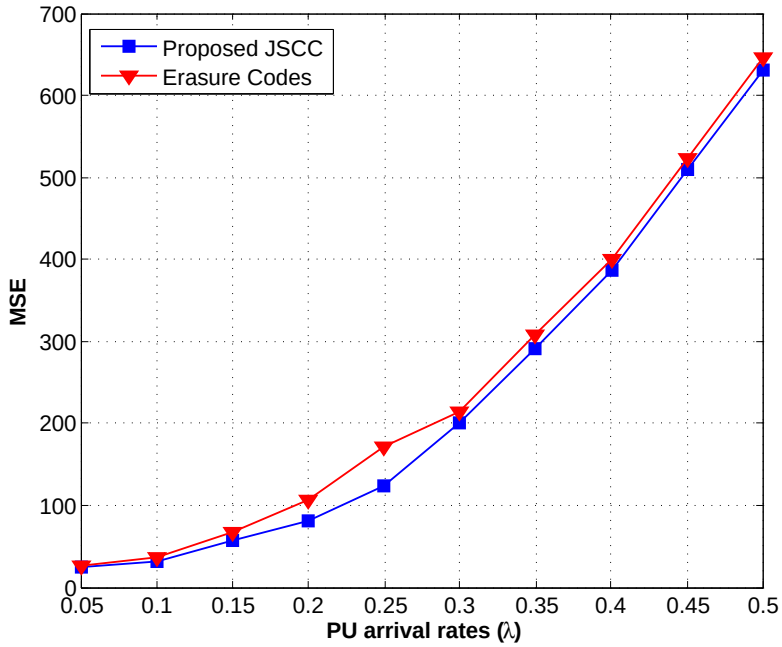

Figure 4.32: Comparison of MSE using JSCC and erasure codes for the transmission of Lena image with transform coding.

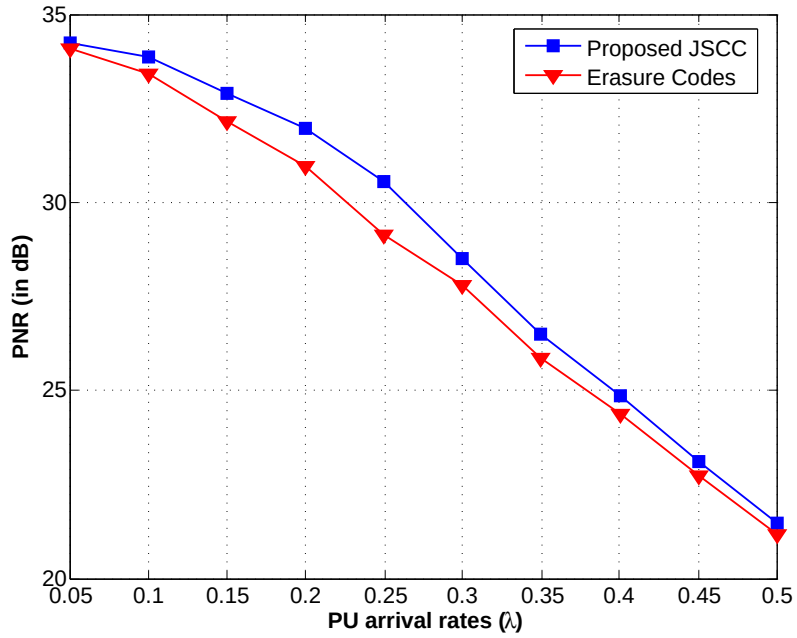

Figure 4.33: Comparison of PSNR using JSCC and erasure codes for the transmission of Lena image with transform coding.

(a) JSCC

(b) Erasure Codes

Figure 4.34: Reconstructed image of Lena at $\lambda = 0.20$ for JSCC and erasure codes.

(a) JSCC

(b) Erasure Codes

Figure 4.35: Reconstructed image of Lena at $\lambda = 0.35$ for JSCC and erasure codes.

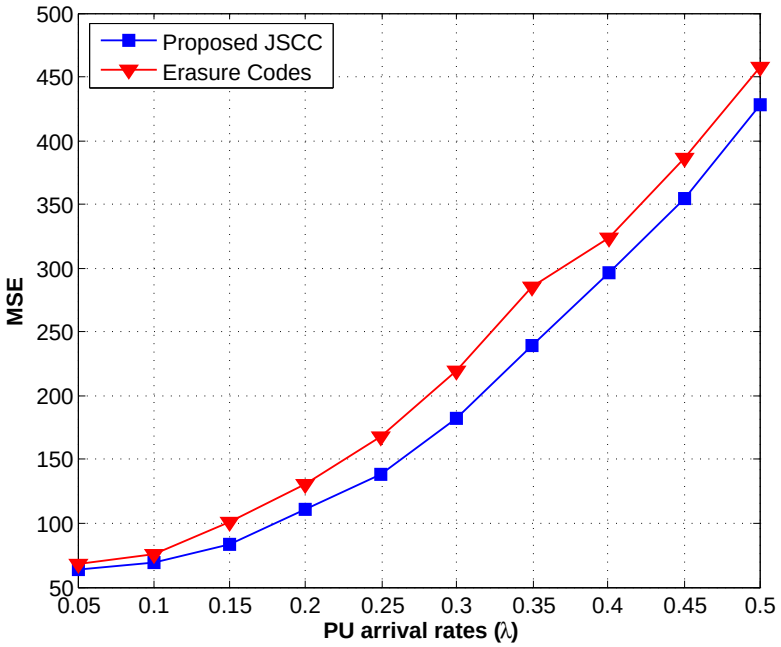

Figure 4.36: Comparison of MSE using JSCC and erasure codes for the transmission of Mandrill image with transform coding.

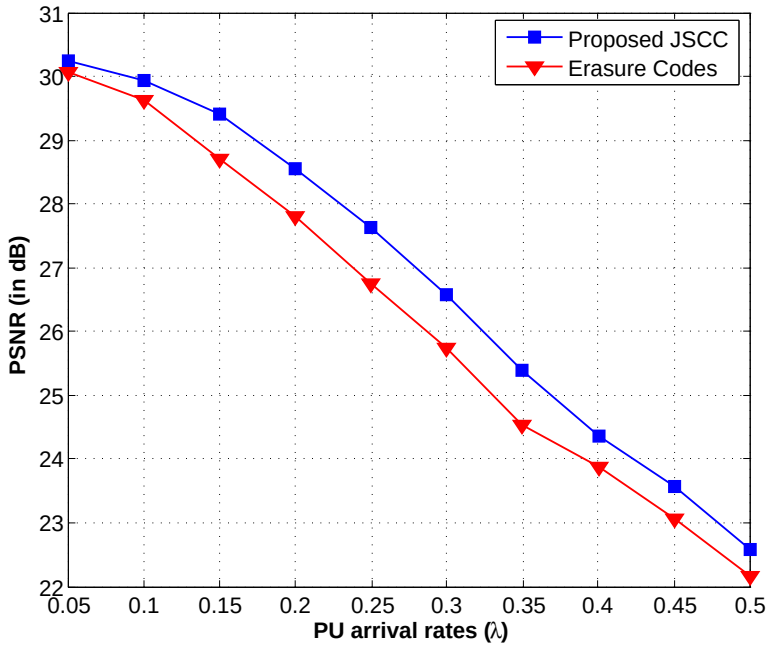

Figure 4.37: Comparison of PSNR using JSCC and erasure codes for the transmission of Mandrill image with transform coding.

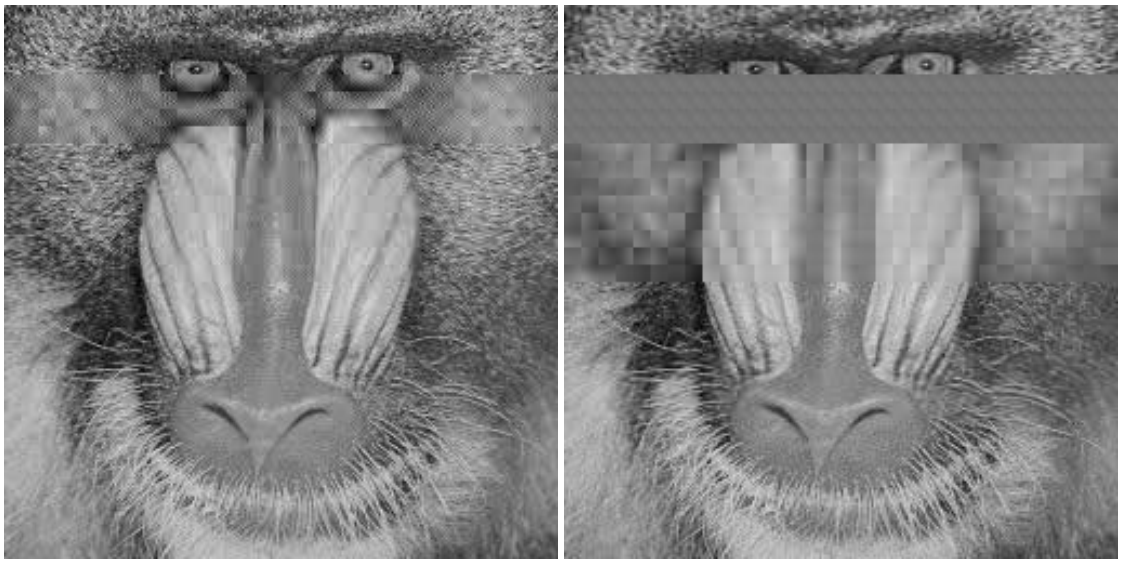

(a) JSCC **(b)** Erasure Codes

Figure 4.38: Reconstructed image of Mandrill at $\lambda = 0.35$ for JSCC and erasure codes.

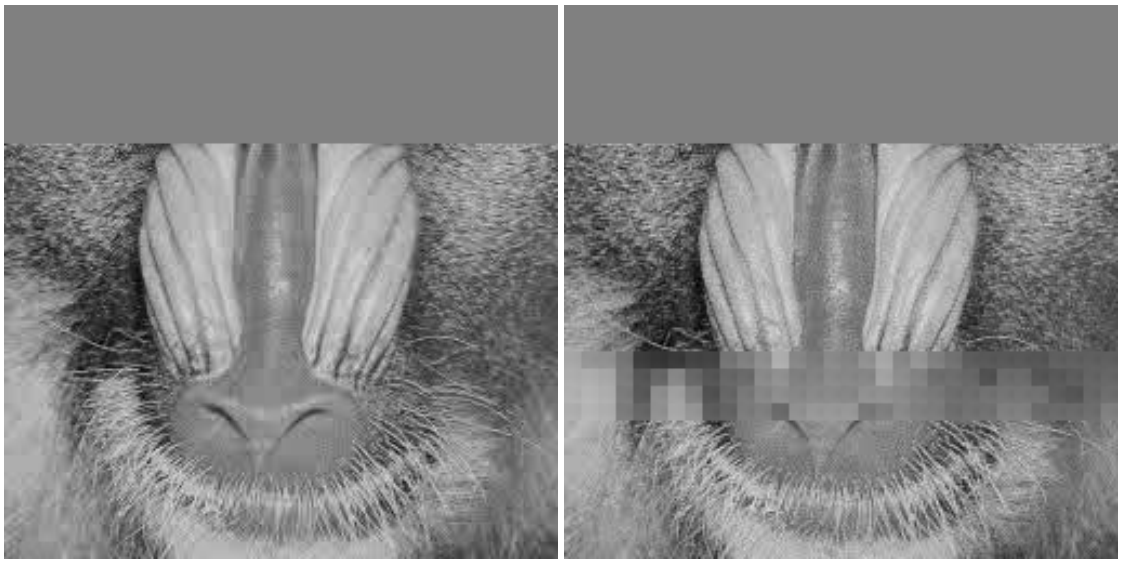

(a) JSCC **(b)** Erasure Codes

Figure 4.39: Reconstructed image of Mandrill at $\lambda = 0.50$ for JSCC and erasure codes.

Chapter 5

Conclusions and Future Work

With radio spectrum becoming a scarce resource, cognitive radio paves a potential solution for spectrum re-use. Recent developments in cognitive radio have motivated the work presented here. This thesis develops an adaptive JSCC for the reliable transmission of SU real-time multimedia. The proposed JSCC uses quantized frame expansion to produce multiple codewords of the source vectors to compensate for the losses incurred by PU arrivals. It is adaptive in the sense that the codewords produced for transmission are adapted to the vacant PU channel conditions and the resolution at which the source is represented is adapted to the available bit rate. It also facilitates the code optimization independently at the transmitter and the receiver eliminating the need of overhead information in SU transmissions. Moreover, this thesis also presented a new bit allocation algorithm which finds a simple solution that can be incorporated into the JSCC design.

Linear reconstruction was used at the decoder in this thesis. *Consistent estimates* [30] can be produced using linear programming or quadratic programming [59], recursive estimation [60] and projection onto convex sets (POCS) [61] which could lower the distortion and help achieve better performance. Dithered quantizer [62] would also help lower the distortion as it would allow the quantization noise to be uncorrelated. The performance could also be enhanced if the coefficients being packed in a BOV were interleaved, thereby, elminating blocks of continuous grey areas at the decoder.

Possible future work

In this thesis, we have explored the real time transmission of Gaussian sources and images. Since the constraints imposed for the transmission of these sources were equaivalent to the conditions for transmission of audio and video signals, it paves a possible pathway for applying the proposed JSCC to audio and video transmissions. Additionally the analysis studied in this thesis could be extended to other PU arrival models like Markov process.

Bibliography

[1] V. Goyal, "Beyond traditional transform coding," Ph.D. dissertation, University of California, Berkeley, December 1998.

[2] C. E. Shannon, "A mathematical theory of communication," *The Bell System Technical Journal*, vol. 27, pp. 379–423, 623–656, July, October 1948. [Online]. Available: http://cm.bell-labs.com/cm/ms/what/shannonday/shannon1948.pdf

[3] FCC, "Spectrum policy task force report, ET Docket No. 02-155," 2002.

[4] M. A. McHenry, P. A. Tenhula, D. McCloskey, D. A. Roberson, and C. S. Hood, "Chicago spectrum occupancy measurements & analysis and a long-term studies proposal," in *Proceedings of the First International Workshop on Technology and Policy for Accessing Spectrum*, ser. TAPAS '06. New York, NY, USA: ACM, 2006. [Online]. Available: http://doi.acm.org/10.1145/1234388.1234389

[5] S. Haykin, "Cognitive radio: brain-empowered wireless communications," *IEEE Journal on Selected Areas in Communications*, vol. 23, no. 2, pp. 201–220, Feb 2005.

[6] R. Tandra, S. Mishra, and A. Sahai, "What is a spectrum hole and what does it take to recognize one?" *Proceedings of the IEEE*, vol. 97, no. 5, pp. 824–848, May 2009.

[7] J. Mitola and J. Maguire, G.Q., "Cognitive radio: making software radios more personal," *IEEE Personal Communications*, vol. 6, no. 4, pp. 13–18, 1999.

[8] A. Goldsmith, S. Jafar, I. Maric, and S. Srinivasa, "Breaking spectrum gridlock with cognitive radios: An information theoretic perspective," *Proceedings of the IEEE*, vol. 97, no. 5, pp. 894–914, May 2009.

[9] B. Gudmundson, J. Skold, and J. Ugland, "A comparison of cdma and tdma systems," in *Vehicular Technology Conference, 1992, IEEE 42nd*, May 1992, pp. 732–735 vol.2.

[10] H. Kushwaha, Y. Xing, R. Chandramouli, and H. Heffes, "Reliable multimedia transmission over cognitive radio networks using fountain codes," *Proceedings of the IEEE*, vol. 96, no. 1, pp. 155–165, Jan 2008.

[11] N. Demir and K. Sayood, "Joint source/channel coding for variable length codes," in *Data Compression Conference, 1998. DCC '98. Proceedings*, Mar 1998, pp. 139–148.

[12] V. Goyal, "Multiple description coding: compression meets the network," *IEEE Signal Processing Magazine*, vol. 18, no. 5, pp. 74–93, 2001.

[13] H. S. Witsenhausen, "On source networks with minimal breakdown degradation," *Bell System Technical Journal*, vol. 59, no. 6, pp. 1083–1087, 1980. [Online]. Available: http://dx.doi.org/10.1002/j.1538-7305.1980.tb03048.x

[14] V. Goyal and J. Kovacevic, "Generalized multiple description coding with correlating transforms," *IEEE Transactions on Information Theory*, vol. 47, no. 6, pp. 2199–2224, Sep 2001.

[15] R. E. Blahut, *Theory and practice of error control codes*. Reading, MA: Addison-Wesley, 1983.

[16] V. Goyal, J. Kovacevic, and M. Vetterli, "Quantized frame expansions as source-channel codes for erasure channels," in *Data Compression Conference, 1999. Proceedings. DCC '99*, Mar 1999, pp. 326–335.

[17] N. Gogate, D.-M. Chung, S. Panwar, and Y. Wang, "Supporting image and video applications in a multihop radio environment using path diversity and multiple description coding," *IEEE Transactions on Circuits and Systems for Video Technology*, vol. 12, no. 9, pp. 777–792, Sep 2002.

[18] H. Li, "Multiple description source coding for cognitive radio systems," in *Cognitive Radio Oriented Wireless Networks Communications (CROWNCOM), 2010 Proceedings of the Fifth International Conference on*, June 2010, pp. 1–5.

[19] E. Dynkin, "Markov processes as a tool in field theory," *Journal of Functional Analysis*, vol. 50, no. 2, pp. 167 – 187, 1983. [Online]. Available: http://www.sciencedirect.com/science/article/pii/0022123683900666

[20] D. Willkomm, J. Gross, and A. Wolisz, "Reliable link maintenance in cognitive radio systems," in *New Frontiers in Dynamic Spectrum Access Networks, 2005. DySPAN 2005. 2005 First IEEE International Symposium on*, Nov 2005, pp. 371–378.

[21] R. W. Brodersen, A. Wolisz, D. Cabric, and S. M. Mishra, "Corvus: A cognitive radio approach for usage of virtual unlicensed spectrum," 2004.

[22] T. Weiss and F. Jondral, "Spectrum pooling: an innovative strategy for the enhancement of spectrum efficiency," *IEEE Communications Magazine*, vol. 42, no. 3, pp. S8–14, Mar 2004.

[23] M. Luby, "Lt codes," in *Foundations of Computer Science, 2002. Proceedings. The 43rd Annual IEEE Symposium on*, 2002, pp. 271–280.

[24] J. F. C. Kingman, *Poisson processes*, ser. Oxford Studies in Probability. New York: The Clarendon Press Oxford University Press, 1993, vol. 3, oxford Science Publications.

[25] J. W. Byers, M. Luby, M. Mitzenmacher, and A. Rege, "A digital fountain approach to reliable distribution of bulk data," *SIGCOMM Comput. Commun. Rev.*, vol. 28, no. 4, pp. 56–67, Oct. 1998. [Online]. Available: http://doi.acm.org/10.1145/285243.285258

[26] A. Chaoub, E. I. Elhaj, and J. E. Abbadi, "Multimedia traffic transmission over cognitive radio networks using multiple description coding." in *ACC (1)*, ser. Communications in Computer and Information Science, A. Abraham, J. L. Mauri, J. F. Buford, J. Suzuki, and S. M. Thampi, Eds., vol. 190. Springer, 2011, pp. 529–543. [Online]. Available: http://dblp.uni-trier.de/db/conf/acc/acc2011-1.html#ChaoubEA11

[27] A. Said and W. Pearlman, "A new, fast, and efficient image codec based on set partitioning in hierarchical trees," *IEEE Transactions on Circuits and Systems for Video Technology*, vol. 6, no. 3, pp. 243–250, Jun 1996.

[28] A. Albanese, J. Blomer, J. Edmonds, M. Luby, and M. Sudan, "Priority encoding transmission," *IEEE Transactions on Information Theory*, vol. 42, no. 6, pp. 1737–1744, Nov 1996.

[29] D. Han, K. Kornelson, D. Larson, and E. Weber, *Frames for Undergraduates*, ser. Student Mathematical Library. Providence, RI: American Mathematical Society, 2007, vol. 40.

[30] V. K. Goyal, J. Kovaevi, and J. A. Kelner, "Quantized frame expansions with erasures," *Applied and Computational Harmonic Analysis*, vol. 10, no. 3, pp. 203 – 233, 2001. [Online]. Available: http://www.sciencedirect.com/science/article/pii/S1063520300903403

[31] V. Goyal, M. Vetterli, and J. Kovacevic, "Multiple description transform coding: robustness to erasures using tight frame expansions," in *1998. Proceedings. 1998 IEEE International Symposium on Information Theory*, Aug 1998, pp. 408–.

[32] S. Mehrotra and P. Chou, "On optimal frame expansions for multiple description quantization," in *2000. Proceedings. IEEE International Symposium on Information Theory*, 2000, pp. 176–.

[33] V. Vaishampayan, "Design of multiple description scalar quantizers," *IEEE Transactions on Information Theory*, vol. 39, no. 3, pp. 821–834, 1993.

[34] A. Gersho and R. M. Gray, *Vector quantization and signal compression*. Kluwer Academic Publishers, 1992.

[35] Z. Wang and A. Bovik, "Mean squared error: Love it or leave it? a new look at signal fidelity measures," *IEEE Signal Processing Magazine*, vol. 26, no. 1, pp. 98–117, 2009.

[36] W. R. Bennett, "Spectra of Quantized Signals," *Bell Systems Technical Journal*, vol. 27, no. 3, pp. 446–472, Jul. 1948. [Online]. Available: http://www.alcatel-lucent.com/bstj/vol27-1948/articles/bstj27-3-446.pdf

[37] B. Oliver, J. Pierce, and C. Shannon, "The philosophy of pcm," *Proceedings of the IRE*, vol. 36, no. 11, pp. 1324–1331, Nov 1948.

[38] S. Lloyd, "Least squares quantization in PCM," *IEEE Transactions on Information Theory*, vol. 28, no. 2, pp. 129 – 137, Mar. 1982.

[39] L. Davisson, "Rate-distortion theory and application," *Proceedings of the IEEE*, vol. 60, no. 7, pp. 800–808, July 1972.

[40] R. Gray and D. Neuhoff, "Quantization," *IEEE Transactions on Information Theory*, vol. 44, no. 6, pp. 2325–2383, 1998.

[41] T. M. Cover and J. A. Thomas, *Elements of Information Theory*. New York, NY, USA: Wiley-Interscience, 1991.

[42] A. Gyorgy and T. Linder, "Optimal entropy-constrained scalar quantization of a uniform source," *IEEE Transactions on Information Theory*, vol. 46, no. 7, pp. 2704–2711, Nov 2000.

[43] A. Renyi, "On the dimension and entropy of probability distributions," *Acta Mathematica Hungarica*, vol. 10, pp. 193–215, 1959.

[44] A. Gamal and T. Cover, "Achievable rates for multiple descriptions," *IEEE Transactions on Information Theory*, vol. 28, no. 6, pp. 851–857, Nov 1982.

[45] R. J. Duffin and A. C. Schaeffer, "A class of nonharmonic Fourier series," vol. 72, pp. 341–366, 1952.

[46] R. A. Horn and C. R. Johnson, *Matrix Analysis*. Cambridge University Press, 1990.

[47] F. Hernández-Campos, M. Karaliopoulos, M. Papadopouli, and H. Shen, "Spatio-temporal modeling of traffic workload in a campus wlan," in *Proceedings of the 2Nd Annual International Workshop on Wireless Internet*, ser. WICON '06. New York, NY, USA: ACM, 2006. [Online]. Available: http://doi.acm.org/10.1145/1234161.1234162

[48] S. Geirhofer, L. Tong, and B. Sadler, "A measurement-based model for dynamic spectrum access in wlan channels," in *IEEE Military Communications Conference*. IEEE, 2006.

[49] S. M. Kay, *Fundamentals of statistical signal processing : estimation theory.*, 1st ed. Prentice-Hall PTR, Apr. 2010.

[50] M. Haleem and R. Chandramouli, "Adaptive downlink scheduling and rate selection: a cross-layer design," *IEEE Journal on Selected Areas in Communications*, vol. 23, no. 6, pp. 1287–1297, June 2005.

[51] Q. Zhao and B. Sadler, "A survey of dynamic spectrum access," *IEEE Signal Processing Magazine*, vol. 24, no. 3, pp. 79–89, May 2007.

[52] S. Huang, X. Liu, and Z. Ding, "Opportunistic spectrum access in cognitive radio networks," in *INFOCOM 2008. The 27th Conference on Computer Communications. IEEE*, April 2008, pp. –.

[53] V. Goyal, J. Zhuang, and M. Veiterli, "Transform coding with backward adaptive updates," *Information Theory, IEEE Transactions on*, vol. 46, no. 4, pp. 1623–1633, Jul 2000.

[54] N. Ahmed, T. Natarajan, and K. Rao, "Discrete cosine transform," *IEEE Transactions on Computers*, vol. C-23, no. 1, pp. 90–93, Jan 1974.

[55] "AES recommended practice for professional digital audio - preferred sampling frequencies for applications employing pulse-code modulations," *AES5-2008*, 2008.

[56] C. Stevenson, G. Chouinard, Z. Lei, W. Hu, S. Shellhammer, and W. Caldwell, "IEEE 802.22: The first cognitive radio wireless regional area network standard," *IEEE Communications Magazine*, vol. 47, no. 1, pp. 130–138, January 2009.

[57] S. Baset and H. Schulzrinne, "An analysis of the skype peer-to-peer internet telephony protocol," in *INFOCOM 2006. 25th IEEE International Conference on Computer Communications. Proceedings*, April 2006, pp. 1–11.

[58] CISCO, "Fundamentals of digital video."

[59] V. Goyal, M. Vetterli, and N. Thao, "Quantized overcomplete expansions in R^N: analysis, synthesis, and algorithms," *IEEE Transactions on Information Theory*, vol. 44, no. 1, pp. 16–31, Jan 1998.

[60] H. Q. Nguyen, V. K. Goyal, and L. R. Varshney, "Frame permutation quantization," *CoRR*, vol. abs/0909.1599, 2009.

[61] P. Chou, S. Mehrotra, and A. Wang, "Multiple description decoding of overcomplete expansions using projections onto convex sets," in *Data Compression Conference, 1999. Proceedings. DCC '99*, Mar 1999, pp. 72–81.

[62] R. Gray and J. Stockham, T.G., "Dithered quantizers," *IEEE Transactions on Information Theory*, vol. 39, no. 3, pp. 805–812, May 1993.